UNIVERSITY OF OKLAHOMA

GRADUATE COLLEGE

NUMERICAL MECHANISTIC STUDY OF IN-SITU CO_2 EOR – KINETICS AND RECOVERY PERFORMANCE ANALYSIS

A THESIS

SUBMITTED TO THE GRADUATE FACULTY

In partial fulfillment of the requirement for the

Degree of

MASTER OF SCIENCE

By

SADAM HUSSAIN

Norman, Oklahoma

2021

NUMERICAL MECHANISTIC STUDY OF IN-SITU CO_2 EOR – KINETICS AND RECOVERY PERFORMANCE ANALYSIS

A THESIS APPROVED FOR THE

MEWBOURNE SCHOOL OF PETROLEUM AND GEOLOGICAL ENGINEERING

BY THE COMMITTEE CONSISTING OF

Dr. Xingru Wu, Chair

Dr. Bor-Jier (Ben) Shiau

Dr. Ali Ousseini Tinni

Acknowledgments

I would first like to extend my hearty gratitude for my advisor Dr. Xingru Wu of the Mewbourne School of Petroleum and Geological Engineering for the continuous support and guidelines during my master study and research. I am thankful for his patience, enthusiasm, and forefront knowledge. Despite the COVID-19 challenges, he was always available for an online meeting whenever I had any question and difficulty in my research. He motivated me to research modeling the synergetic mechanisms in in-situ CO_2 enhancing oil recovery. He did not only guide me on my research but also gave me some helpful suggestions for the future career.

I would also like to thank my thesis committee members, Dr. Bor-Jier (Ben) Shiau and Dr. Ali Ousseini Tinni from Mewbourne School of Petroleum and Geological Engineering. For their encouragement and insightful comments on this research.

Last but not the least, I must express my very profound gratitude to my parents, my wife Romana Sadam, and my kids Muhammad Ibrahim and Aiza to support me and continuous encouragement throughout my years of study. Love you forever.

Table of Contents

List of Figures

List of Tables

Abstract

The success of supercritical CO_2 Enhanced Oil Recovery (EOR) cannot be duplicated if the cost of CO_2 transposition and processing becomes prohibitive. Research results of the in-situ CO_2 EOR (ICE) approach offered a potential technology for many waterflooded stripper wells that lack access to affordable CO_2 sources. Previously the ICE synergetic mechanisms were only qualitatively attributed to oil swelling and viscosity reduction due to the preferential partition of CO_2 into the oleic phase. This study aims to quantify the contributions to recovery factors from several plausible mechanisms with numerical modeling and simulation.

First, urea reaction was modeled as the CO_2 generating chemical decomposing to CO_2 and ammonia under the reservoir conditions. The CO_2 partitions into oil, which leads to the reaction continuation to generate more CO_2. The resulting ammonia largely left in water may further react with certain oil components to generate surfactant, thus decreasing the oil/water interfacial tension (IFT). It is expected that the oil containing CO_2 also has a lower IFT with water. The reaction kinetics under different temperatures were incorporated into the model. A numerical model featuring the synergetic mechanisms was built, including stoichiometry and kinetics of urea reaction, oil swelling effect, oil viscosity reduction, and IFT reduction effect on the relative permeabilities. I matched previous laboratory data for three different oils including dodecane, Earlsboro oil, and DeepStar oil, the same oils used in laboratory studies. The phase behavior was modeled with the Equation of State (EOS) under different mole fractions of CO_2.

The estimated reduction of oil viscosity was calculated, 79% for Earlsboro oil, 91% in DeepStar oil, and 76% in dodecane oil. The oil swelling factors ranged from 10% to 50% in the three lab models, which translate to the recovery factor of oil. Then I modified the endpoints of relative

permeability to account for the recovery contribution to the IFT and viscosity reduction. The impact of reaction kinetics on oil swelling and recovery factor was also determined, and they are not numerically close to reaction kinetics which were used in the lab cases. The study concluded that the incremental recovery due to oil swelling ranges between 6.4% and 18.0%, and the from 24% to 38% is due to IFT and viscosity reduction for all the cases. The relative permeability and urea reaction kinetics remained the most uncertain parameters during history matching and modeling the ICE synergetic mechanisms. Later on, I upscaled the lab-scale model to a 3D sector model which features reaction kinetics, multi-components, and sensitivity study on selected parameters.

To my knowledge, this is the first in modeling and differentiating the individual contributions on recovery from the synergetic mechanisms of ICE. The success of this model will tremendously reduce the potential laboratory experiment efforts and significantly improve the modeling capability in field application of the ICE technology. The developed model can be easily upscaled and retrofitted for other applications such as development planning and production forecast for ICE.

Chapter 1: Introduction

1.1. Overview

The world's energy demand is increasing day by day, and the share of oil and gas in global energy consumption is 33.10% and 24.20%, respectively [1]. The consumption of oil rose by 0.9% in 2019 and this growth was mainly caused by the oil consumption increase in China and other developing countries [1]. In 2019, about 60,000 bbl/day decrease in global oil production was also observed [1]. Figure 1-1 shows the shares of global primary energy percentage. The major share of oil production comes from conventional oil reservoirs except for the United States. In the U.S., 63% of oil production came from unconventional (tight/shale) oil reservoirs in 2019 [2]. The tight or unconventional oil reservoirs are the low-permeability oil reservoirs embedded in shale, carbonate, and sandstone formations.

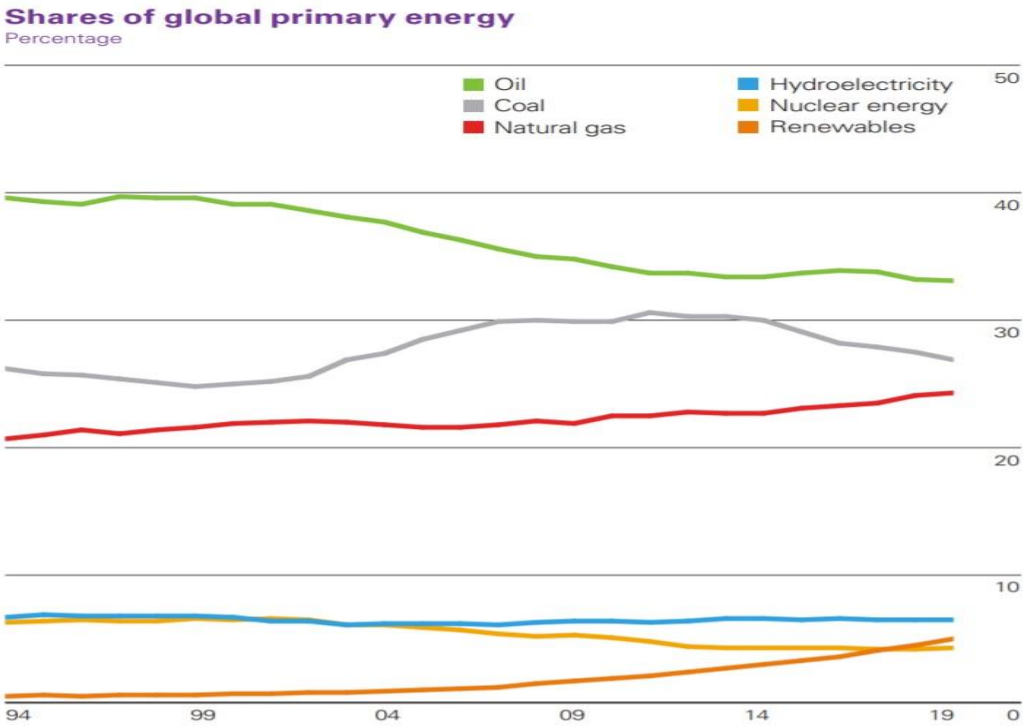

Figure 1-1 Global primary energy percentage from 1994 to 2019 [1]

To meet the increasing demand for energy, production from conventional and unconventional oil reservoirs must be enhanced. Production from oil reservoirs can be enhanced by injecting different fluids and changing the properties of reservoir fluid and reservoir rock. Enhanced oil recovery (EOR) is one of the techniques used to recover the remaining trapped oil from the reservoir by the injection of fluids. EOR can be classified as miscible/immiscible gas, chemical, and thermal EOR.

The gas EOR is injecting a lean gas mixture or rich gas into a reservoir under specific conditions. The gas injection can be miscible or immiscible depending on injection gas composition and reservoir conditions [3]. If the reservoir pressure is higher than the minimum miscibility pressure (MMP) injected gas will be miscible with reservoir fluid and vice versa. The supercritical CO_2-EOR is the most widely used miscible/immiscible EOR technique in the world [1]. The miscible/immiscible EOR is further explained in chapter 2 Literature Review.

The chemical EOR can be further classified into three main categories, polymer, alkali, and surfactant flooding based on the injection of different chemicals into a reservoir to change the reservoir rock properties. Polymer flooding increases the viscosity of injected fluid (water) to reduce the mobility ratio and thus increases the volumetric and displacement sweep efficiency and results in incremental oil recovery. The oil/water interfacial tension (IFT) is decreased by injecting a surfactant, to displace oil and thus improves the microscopic displacement efficiency. This technique reduces the residual (trapped) oil saturation. The alkali flooding reduces oil/water interfacial tension and residual oil saturation by injecting a high-pH chemical to generate in-situ surfactant (saponification). It also can alter the wettability of the reservoir rock. It is mainly applied to low API crude oils.

This study is a combination of chemical and CO_2-EOR. Due to an increase in oil demand and a reduction in oil prices, EOR has become challenging. During a low oil price environment, the capital investment on the costs of chemicals used in surfactant flooding and costs of infrastructure, processing, and injection of CO_2 has become impossible for the global oil industry. To enhance oil recovery and meet the oil demand, a combination of chemical and CO_2 EOR techniques has been developed, known as In-Situ CO_2 EOR (ICE). ICE produces CO_2 in the reservoir by injecting a CO_2-generating chemical to resolve issues like CO_2 availability, transportation, and infrastructure.

The ICE technique generates CO_2 and ammonia in the reservoir by injecting ammonium carbamate. The ammonium carbamate converts into urea which decomposes into CO_2 and ammonia under reservoir conditions. The related chemical reactions are shown below:

$$NH_2COONH_4 \rightleftarrows NH_2CONH_2 + H_2O \quad \text{..... (1-1)}$$

$$NH_2COONH_2 + H_2O \rightleftarrows 2NH_3 + CO_2 \quad \text{..... (1-2)}$$

Wang [5] has experimentally shown two synergetic mechanisms of ICE, 1) the reaction generated CO_2 partitions into oil, reduces the oil viscosity and swells the oil, and 2) ammonia reacts with water and generates a weak base (pH between 7 to 10) solution which in turn reacts with petroleum acids in the oil to produce in-situ surfactant (saponification). The ammonia solution acts as alkali and reduces oil/water interfacial tension and increases oil relative permeability [5]. Additionally, the generation of CO_2 and ammonia is highly dependent on reservoir temperature and reaction kinetics. Also, Wang [5] has reported an incremental oil recovery of up to 60% by ICE. The synergetic mechanisms of ICE and urea hydrolysis reaction kinetics are discussed in Chapter 2 Literature Review.

1.2. Objectives

This study is based on a numerical simulation approach to model and to quantify In-situ CO_2 EOR (ICE) synergetic mechanisms. The objectives of this research study are:

1. Study of urea hydrolysis
    i. Study and evaluate reaction stoichiometry.
    ii. Study reaction equilibrium, order, and kinetics
    iii. Estimate Gibbs free energy of urea hydrolysis reaction.
2. Build a 1D numerical mechanistic model.
    i. Build a 1D numerical model based on octane as the oleic phase.
    ii. Incorporate urea hydrolysis reaction, stoichiometry, and reaction kinetics in the numerical model.
    iii. Estimate oil (octane) swelling factor based on an equation of state (EOS)
    iv. Evaluate synergetic mechanisms, i.e., oil swelling and viscosity reduction.
    v. Develop a workflow to model the ICE technique.
    vi. Quantify the contributions of two synergetic mechanisms in terms of recovery factors.
3. Update the 1D mechanistic model to history match laboratory experiments of ICE performed by Wang [1]
    i. History match the three laboratory experiments of ICE based on different oil compositions, i.e., dodecane, Earlsboro oil, and DeepStar oil.
    ii. History match oil saturation versus injection pore volume for three laboratory experiments.
    iii. Validate the two synergetic mechanisms for laboratory experiments.

iv. Quantify the contributions of two synergetic mechanisms in terms of recovery factors.

v. Evaluate critical uncertainties in the history matching process.

4. Upscale the 1D mechanistic model to a 3D field-scale simulation model

i. Build a 3D 10-acre quarter 5-spot waterflooding pattern field-scale simulation model.

ii. Use three pseudo-components light component, medium component, and heavy component to simulate oil phase transition in the model (Ref: CMG STARS Template, SPE-003)

iii. Validate two mechanisms, oil swelling and viscosity reduction, and wettability alteration due to ammonia alkali effect.

iv. Perform sensitivity analysis for injection rate, shut-in/no-shut-in, urea concentration, and reservoir temperature.

v. Quantify the contributions of two synergetic mechanisms in terms of recovery factors.

vi. Evaluate the optimized scenario based on sensitivity analysis.

The above-described objectives of the study are based on the criteria of modeling the synergetic mechanism of ICE and are set up with decreasing uncertainty and increasing confidence at each milestone. The objectives are explained in detail in chapter 4 which explains how the numerical models were built, incorporating the urea hydrolysis reaction, and observations in each numerical model scheme.

Chapter 2: Literature Review

2.1. Overview

The oil recovery processes are mainly in three phases: primary, secondary, and tertiary recovery. Approximately 60-70% of the original oil in place (OOIP) cannot be produced by conventional methods in all types of reservoirs [6]. The oil is trapped due to either capillary or viscous forces and reduces the oil displacement by the aqueous phase. Enhanced oil recovery (EOR) is a suite of techniques used to recover trapped oil that cannot be produced during primary and secondary production. It has been estimated that there are currently around 370 EOR projects operating globally, producing just over 2 million barrels per day (MMBbl/d) of oil in 2017 [7]. Figure 2-1 shows the global EOR projects from 1971 to 2017.

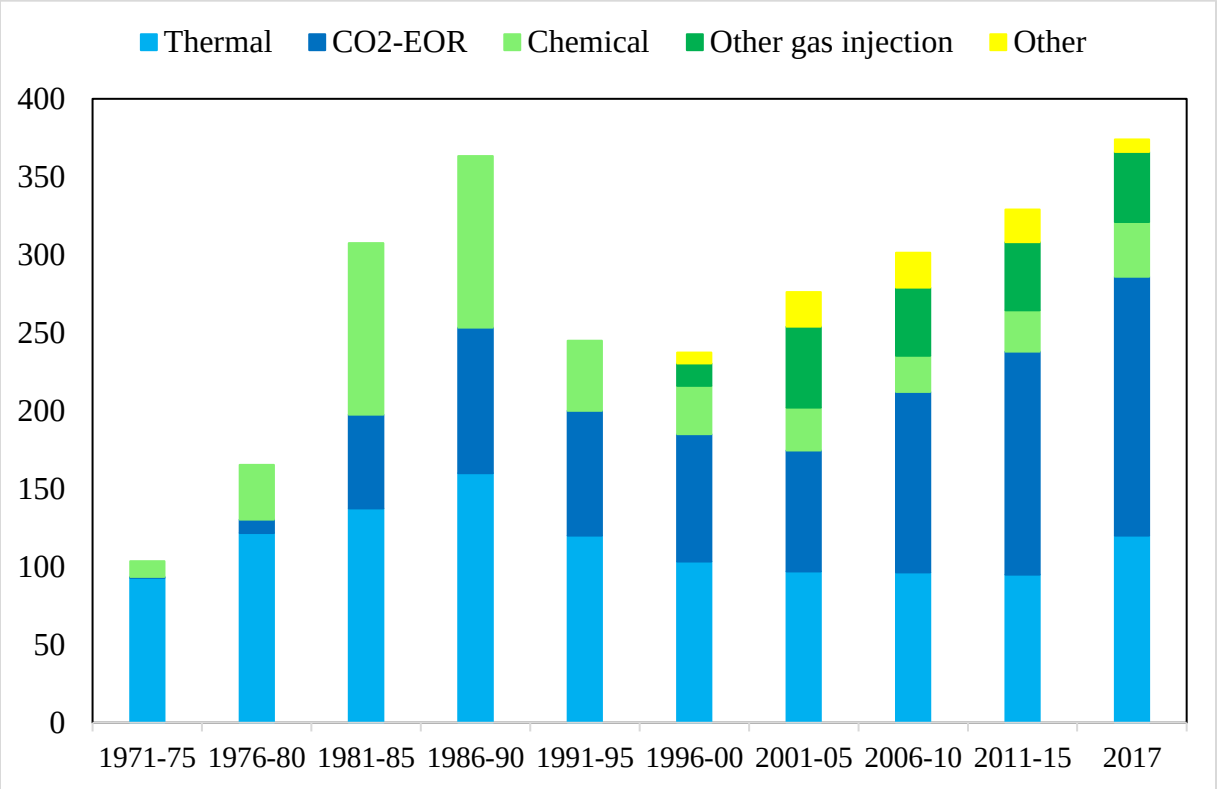

Figure 2-1 Number of EOR projects globally 1971-2017 [7]

The oil displacement efficiency is a combination of macroscopic (volumetric) and microscopic (pore-scale) displacement efficiencies

Macroscopic displacement efficiency measures the efficiency of the injected fluid volumetrically sweeping the oil zone out of the total reservoir volume. The macroscopic efficiency is reflected by overall residual oil saturation (S_{or}). The overall displacement efficiency can be calculated using the equation below:

$$\varepsilon = \varepsilon_D \, \varepsilon_V \ldots\ldots\ldots\ldots\ldots\ldots\ldots\ldots\ldots\ldots \text{(2-1)}$$

where,

ε_D, microscopic displacement efficiency

ε_V, macroscopic (volumetric) displacement efficiency

EOR methods can also be categorized as thermal and non-thermal methods. The non-thermal methods include miscible/immiscible gas and chemical flooding. The thermal methods include steam injection, cyclic steam (huff 'n' puff), in-situ combustion, and hot water injection. The thermal methods are widely applied to heavy oil reservoirs. This study mainly focuses on a combination of chemical EOR and CO_2-EOR.

Chemical EOR methods include surfactant, alkaline, polymer flooding, and a combination of alkali surfactant and polymer (ASP) flooding. In addition to increasing injected fluid viscosity, polymer flooding increases the volumetric and displacement sweep efficiency and results in incremental oil recovery. Polymer gels are also applied to reduce water cut at production wells by blocking or diverting the flow. The mobility ratio is the ratio of injected fluid mobility to the displaced fluid mobility and can be calculated using the equation below:

$$M = \frac{K_w \mu_o}{K_o \mu_w} \text{..... (2-2)}$$

where,

M, the mobility ratio

K_o, the permeability to oil (md)

μ_w , the viscosity of water (cp)

K_w, the permeability to water (cp)

μ_o , the viscosity of oil (cp)

The stability of a displacement method is affected by the mobility ratio (M). If M>1, it indicates water is more mobile than oil and represents unstable flow or non-uniform displacement front because water fingers through the oil that leads to an early water breakthrough. Therefore, it is always desired to have M≤1 for a better volumetric sweep efficiency.

Surfactant flooding is used to decrease the oil/water interfacial tension (IFT) to displace oil and thus improves the microscopic displacement efficiency. This technique can reduce the residual (trapped) oil saturation. The wettability of the reservoir rock is also changed due to surfactant/rock interaction. A surfactant is characterized by two functional groups, hydrophilic (water-soluble) and hydrophobic (oil-soluble) [8]. When a surfactant is injected with water into a reservoir, the hydrophilic part reacts with water, while the hydrophobic part reacts with the crude oil. As a result, an adsorbed film arises that reduces the IFT at the water/oil interface and decreases the capillary forces that allow the trapped oil to flow. The Figure 2-2 showing the surfactant adsorption at water/oil interface.

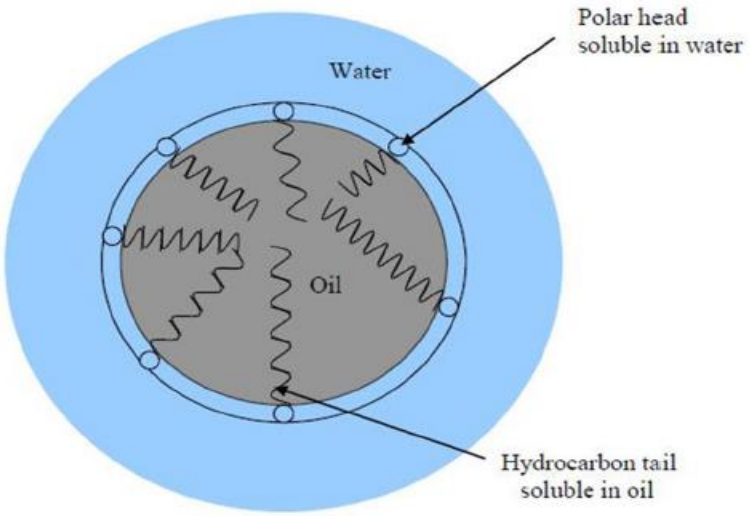

Figure 2-2 The surfactant adsorption at water/oil interface [2]

The alkali flooding reduces oil/water interfacial tension and residual oil saturation by injecting a high-pH chemical to generate in-situ surfactant via saponification. The most used chemicals for alkaline flooding are sodium hydroxide, sodium carbonate, and sodium orthosilicate [9]. The formation of in-situ surfactant is shown in reactions 2-3 and 2-4.

$$HA_w \leftrightarrow H^+ + A^- \quad \text{(2-3)}$$

$$HA_w + OH^- \leftrightarrow A^- + H_2O \quad \text{(2-4)}$$

2.2. Supercritical CO_2 EOR

The CO_2 EOR is one of the most successful techniques applied to recover trapped oil worldwide. The oil production from CO_2 EOR projects accounts for nearly 6% or 350,000 barrels a day of the U.S. oil production [10]. According to the U.S. Department of Energy (DOE), CO_2 EOR can potentially recover up to 137 billion barrels of oil resources and 67 billion barrels can be recovered economically at $85 per barrel [10].

The CO_2 EOR method recovers the remaining oil by improving the microscopic and macroscopic sweep efficiencies. CO_2 EOR works on two major mechanisms, 1) oil swelling; and 2) oil viscosity reduction. Typically, the supercritical CO_2 flooding is a multi-contact process, and under proper conditions, multi-contact miscibility (MCM) can be obtained.

It has been identified that the MCM process is a combination of vaporizing and condensing mechanisms. Initially, the pure CO_2 contacts and vaporizes the reservoir oil by achieving the dynamic miscibility and in-situ vaporization of intermediate hydrocarbons from reservoir oil. After multiple contacts of CO_2 with reservoir oil, the condensation of intermediate hydrocarbons into lean reservoir oil that is vaporized in rich solvent takes place. Figure 2-3 shows the different CO_2 multi-contact miscibility processes in between injection and production wells.

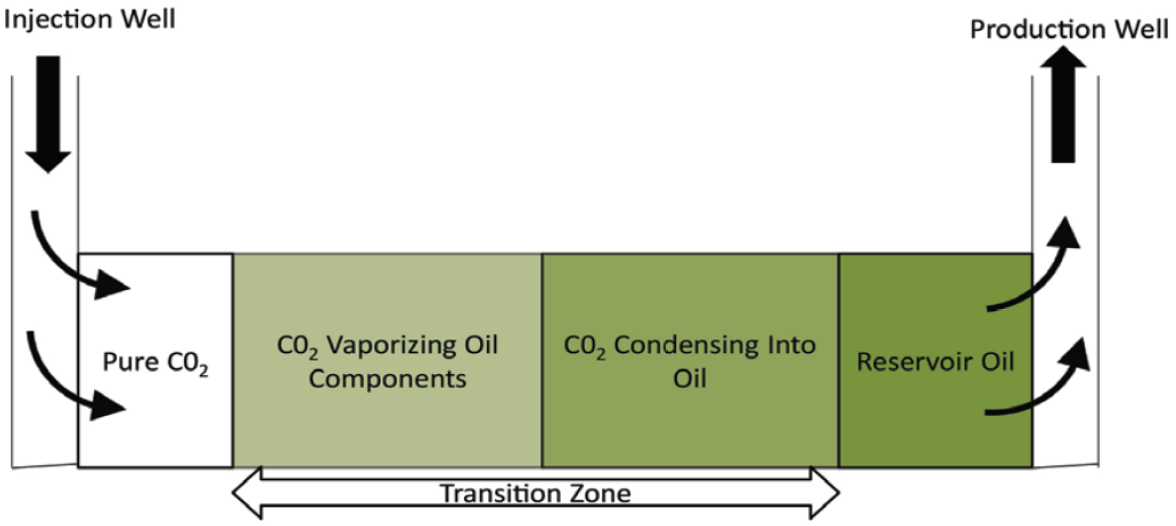

Figure 2-3 Different multi-contact miscibility process in CO_2 EOR [11]

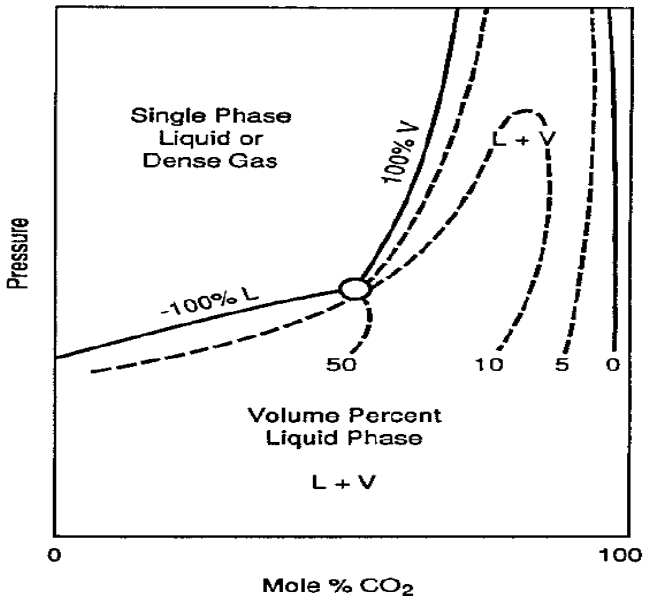

Figure 2-4 CO_2 and hydrocarbon phase behavior at different CO_2 mole fractions [9]

The phase behavior of the CO_2 EOR process is quite complex. It has been observed that adding lighter hydrocarbons components into injected CO_2 can decrease the minimum miscibility pressure. Figure 2-4 shows the phase behavior at different CO_2 mole fractions at a temperature above 120 °F.

In the immiscible displacement process, the microscopic displacement efficiency is generally less than unit compared to the miscible displacement process. In the miscible displacement process, the microscopic displacement efficiency can approach 100% because IFT and capillary pressure diminish.

Even when the CO_2 is not miscible, it still dissolves in the reservoir oil, swells the oil volume, and reduces the oil viscosity. Both will improve displacement efficiencies and increase oil recovery [11]. The CO_2 solubility in the reservoir oil decreases with temperature and increases with pressure as shown in Figure 2-5.

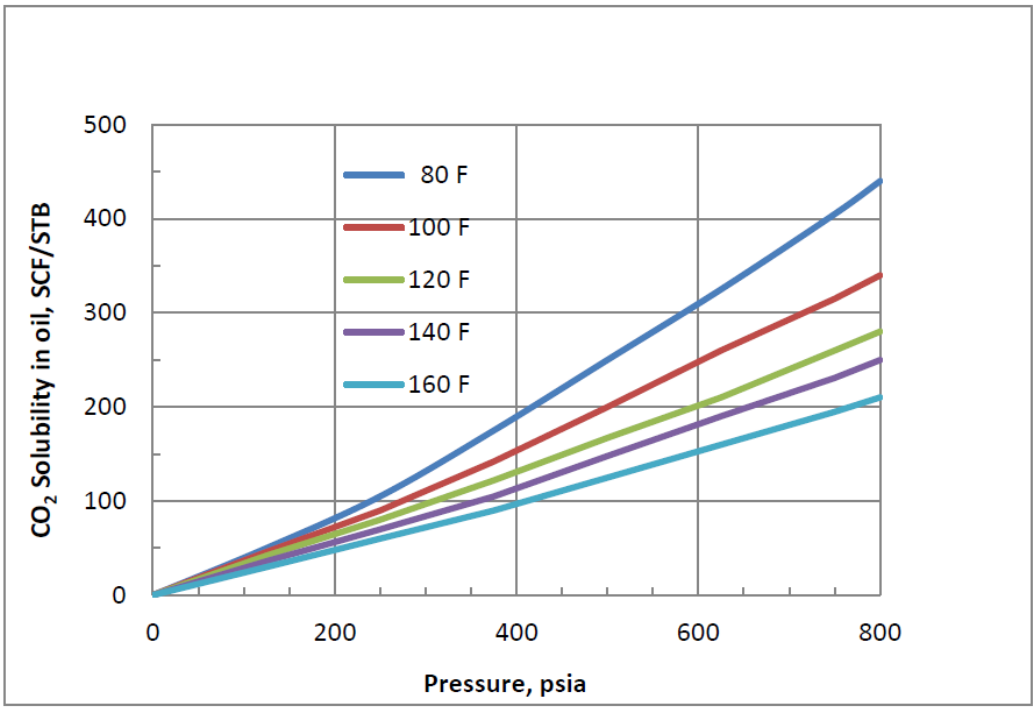

Figure 2-5 CO_2 solubility in the reservoir oil (scf/stb) at different pressures and temperatures. CO_2 solubility reduces with increasing temperature [11]

While the supercritical CO_2 EOR is one of the most effective EOR techniques in conventional reservoirs, some technical and economic challenges are yet to be addressed, such as CO_2 availability and costs of processing. CO_2 EOR requires a vast infrastructure and pipeline network to bring natural resource or human-made resources of CO_2 to oilfields. There are CO_2 pipelines with a total length of over 4,500 miles in the U.S. [12]. These separate pipeline networks are linked with CO_2 resources such as electric powerhouses and industrial sources. However, to increase the oil production from CO_2 EOR projects, the economic limit of CO_2 availability, infrastructure, transportation, and processing must be considered. Due to the cyclic behavior of oil prices, these projects seem to be less attractive because of high capital investment and longer time of capital return. Practically, the capital expenditure for infrastructure and availability of the low-cost CO_2 source is the main economic concern for any CO_2 EOR project.

2.3. In-Situ CO_2 EOR

Research studies at the University of Oklahoma have been conducted to develop a generated solution for in-situ CO_2 EOR at reservoir conditions [5]. A gas generating agent was injected with water that releases CO_2 and ammonia at reservoir conditions. Different gas generating agents such as ammonium carbamate, aluminum carbamide, ammonium bicarbonate, and sodium carbonate have been utilized for ICE [5]. Wang [5] developed a new formulation for ICE that uses CO_2 capture technology products as a gas generating agent. Wang selected ammonium carbamate solution because at a reservoir temperature higher than 70°C, the CO_2 absorbed in the carbamate can be dissociated. This carbamate solution is a salt of monovalent ammonium with the chemical formula NH_2COONH_4. Wang [5] reported that urea was used to produce ammonium carbamate, and this decomposes at reservoir temperature above 60°C. Wang [5] did not report the method by which the temperature of urea decomposition was measured. Therefore, the Gibbs free energy of urea hydrolysis reaction was estimated to quantify the temperature at which urea reaction becomes spontaneous in this study. Urea is very soluble in water, having a solubility of 1079 g/L at 20°C. The essential reactions of urea and ammonium carbamate in the reservoir conditions are shown in Eqn 1-1 and Eqn 1-2.

The reaction in equation 1-1 is exothermic while forming ammonium carbamate due to urea hydrolysis in water. However, the reaction of ammonium carbamate dissociation into carbon dioxide and ammonia is strongly endothermic. These two reactions of in-situ CO_2 generation involve complex chemical processes and are affected by several factors such as reaction activation energy, reaction frequency factor, and reservoir temperature. This new technique has potential advantages over conventional CO_2 EOR/WAG which include [5]:

1. Relaxing the constraints of CO_2-EOR requirement of the natural CO_2 sources, availability, infrastructure, and transportation issues.
2. Enhancing displacement efficiency as compared to CO_2 EOR by partitioning into the oil and reduces oil viscosity.
3. Spontaneous urea reaction with water to generate ammonia and CO_2.
4. The minimal upfront cost for converting from waterflooding to In-Situ CO_2 flooding
5. Sufficient recovery performance above and below MMP.

There are two main recovery mechanisms involved in the ICE process: 1) Oil swelling and viscosity reduction due to CO_2 partitioning; and 2) wetting reversal of the reservoir rock by in-situ generated surfactant. Wang [8] performed several laboratory experiments ICE for different oil compositions and reported the oil recovery up to 60% and residual saturation reduction up to 10% [8]. Figure 2-6 shows the mechanisms of urea generating CO_2 and NH_3 in-situ with and without oil contact.

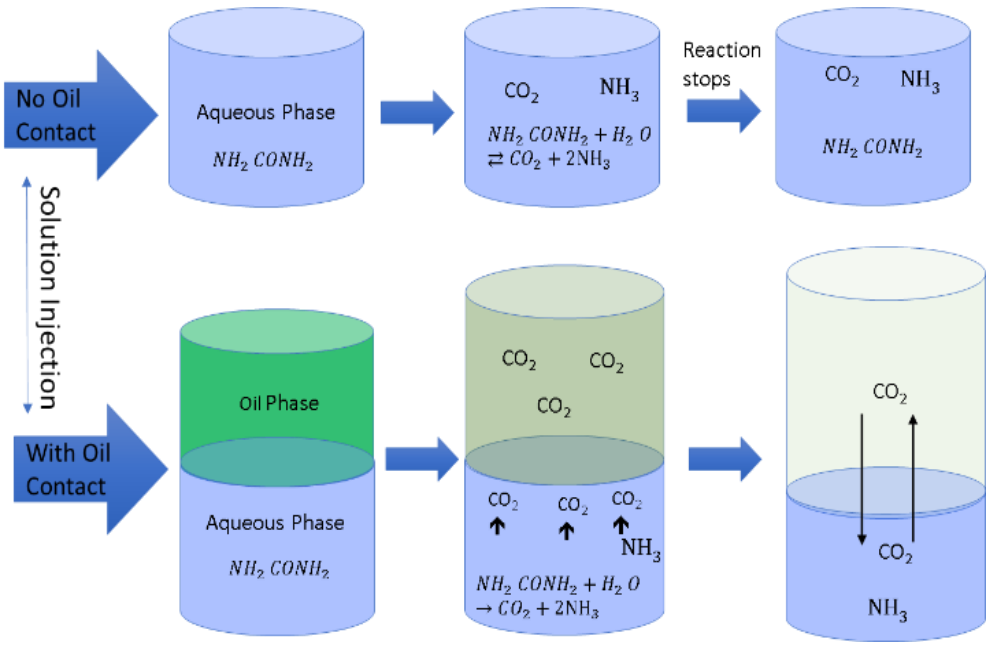

Figure 2-6 The process mechanism of in-situ CO_2 EOR using urea [5]

Wang et al [13] proved that ammonium hydroxide has a quicker induction time to discharge bitumen at the same pH compared to sodium hydroxide. The reaction 2-7 and 2-8 show the generation of in-situ surfactant by ammonium hydroxide:

$$NH_3 + H_2O \rightarrow NH_4^+ + OH^- \quad \text{..... (2-7)}$$

$$HA + OH^- \rightarrow A^- + H_2O \quad \text{..... (2-8)}$$

Where HA is a petroleum acid dissolved in the oleic phase that transfers to oil/water interface and transforms into an anionic surfactant A^- and reduces the IFT. The mechanisms of generation of in-situ surfactant and wettability reversal as an additional benefit of urea injection reduce the IFT and release polar components in the crude oil. Alteration of wettability plays an important role, especially in oil-wet carbonate reservoir rocks during EOR. The carbonate reservoirs are typically neutral to oil-wet due to polar components such as organic acids and asphaltenes in the oil. The polar ends of these components and positive charge of carbonate rock contact each other, and the long-chained hydrocarbon components exhibit loosely to the aqueous phase, and this makes the solid rock surface more oil-wet [14].

2.4. Reaction Characteristics

Every reaction has three characteristics that affect the rate of reaction: chemical equilibrium; reaction kinetics; order of reaction.

2.4.1. Chemical Equilibrium

The chemical equilibrium is a state at which the net rate of change of reactants and product concentrations becomes zero. It is also known as a 'steady-state reaction.' The expression of the equilibrium for a chemical reaction can be stated in terms of concentrations of reactants and

products, and only aqueous and gaseous phases chemical species are involved in the expression of equilibrium. A formal expression of equilibrium is given in 2-9:

$$xA + yB \rightarrow mC + nD \quad \text{(2-9)}$$

The equilibrium constant can be expressed as below:

$$K_{eq} = \frac{([C]^m[D]^n)}{([A]^x[B]^y)} \quad \text{(2-10)}$$

Where K_{eq} is the equilibrium constant and [A], [B], [C], [D] are the molar concentrations of reactants and products. x, y, m, n are the coefficients of the reactants and products. It can also be expressed in terms of free energy (kJ/mol) and is given below in 2-11.

$$K_{eq} = e^{-\Delta G^o/RT} \quad \text{(2-11)}$$

Where ΔG^o is the standard free energy (kJ/mol), R is the universal gas constant (0.00831447 kJ/mol.K), and T is the temperature (Kelvin). The determined standard free energy of urea hydrolysis reaction is 13.47 kJ/mol. The factors which affect the chemical equilibrium are:

i. The chemical concentration of reactants and products
ii. Pressure and temperature of the system
iii. Adding a catalyst in the system

According to Le-Chatelier's principle, any changes in the factors that affect the conditions of chemical equilibrium, the overall conversion of the system will be reduced or counteracted.

2.4.2. Order of Reaction

The order of a reaction is the relationship between the reaction rate and concentrations of different species [16]. The order of rate is defined as the sum of the exponents of concentration.

In other words, the order of a reaction is the exponent to the concentration of that species is raised, and it shows the extent of concentration of a species that influences the rate of reaction. For a simple reaction given in 2-12, the rate law is given in 2-13:

$$xA + yB \rightarrow C \quad \text{..... (2-12)}$$

$$\text{rate} = k\,[A]^a[B]^b \text{.....} \quad \text{(2-13)}$$

Where A and B are the concentrations of species A and B (mol/dm^3), a and b are the order of species A and B, k is the rate constant, and the rate is the rate of reaction (mol/dm^3.s). The total order of a reaction is n, which is the sum of the order of reaction of reactants A and B. Therefore:

$$n = a + b \quad \text{..... (2-14)}$$

It is not necessary for an order of reaction to be an integer, and the order of reaction can be [12]:

- Zero means that the rate of reaction is not affected by the concentration of reaction species.
- Negative indicates that the rate of reaction is inversely affected by the concentration of species.
- Positive implies that the rate of reaction is directly affected by the concentration of species.
- Non-Integer, both negative and positive non-integer orders show that the reaction rate is complex and the relationship between concentrations is more complicated.

Sahu et al. [17] reported the order and rate of reaction of urea hydrolysis by experimentally measuring the values of the final concentration of urea solution. They proved that urea hydrolysis is a forward first-order type reaction; the reaction order is close to 1, and the forward

rate constant is a function of temperature. It was determined that the rate constant increases from 0.013 to 0.22 min^{-1} with increases in temperature from 140°C to 150°C [17]. The rate of reaction was computed as given in 2-15 and 2-16:

$$-r_A = \frac{-dC_A}{dt} = k\,(C_A)^n \quad \text{..... (2-15)}$$

Taking log on both sides of the equation gives:

$$\ln(-r_A) = \ln(k) + nln(C_A) \quad \text{.....(2-16)}$$

Where r_A is the rate of reaction, C_A is the concentration of urea solution at any time, k is the rate constant, and n is the forward reaction order. Figure 2-7 shows the relationship between the reaction rate and the final concentration of urea solution at different temperatures.

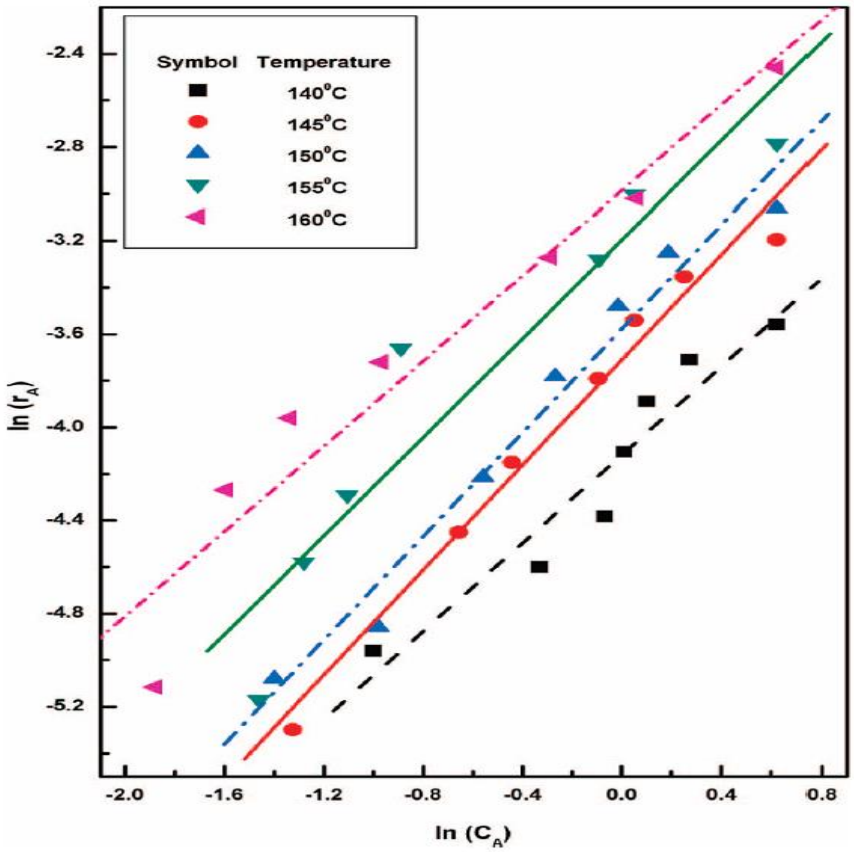

Figure 2-7 Changes in urea concentrations and reaction rate and different temperatures [17]

2.4.3. Reaction Kinetics

Chemical reaction kinetics [15] provides the rates of conversion of chemical compounds from reactant species into products. During urea hydrolysis, the reaction rate and generation of the desired CO_2 and NH_3 moles are controlled by the reaction kinetics. Based on Arrhenius theory of reaction kinetics, the dependence of temperature on the rate constant can be explained and shown in 2-17:

$$k = Ae^{-E_a/(RT)} \quad \text{..... (2-17)}$$

Where k is the reaction rate constant (min^{-1}), A is the pre-exponential factor (min^{-1}), E_a is the activation energy (kJ/mol), R is the universal gas constant (kJ/mol·K), and T is the absolute temperature (K). Wang et al. [5,18] measured the reaction rate constant at different temperatures and computed the urea reaction activation energy as 94.26 kJ/mol and pre-exponential factor (reaction frequency factor) as 1.7E+09 min^{-1}. It was observed that urea hydrolysis was very slow at temperatures below 70°C. Therefore, he added 1 wt.% NaOH to increase urea decomposition and measured the reaction rate constant. The activation energy and pre-exponential factor with 1 wt.% NaOH was 86.84 kJ/mol and 3.3E+08 min^{-1}. Sahu et al. [17] and Kieke et al. [19] also reported the reaction kinetics of urea hydrolysis at different temperatures. The different values of activation energy and pre-exponential factor by different researchers [8,13, 14, 15] are different due to unlike experimental methods, but they concluded that urea decomposition is very slow when the temperature is below 70°C. Figure 2-8 shows the reaction rate constants at different temperatures reported by previous researchers [5, 17, 18, 19]. The activation energy and pre-exponential factor by different authors are provided in Table 2-1.

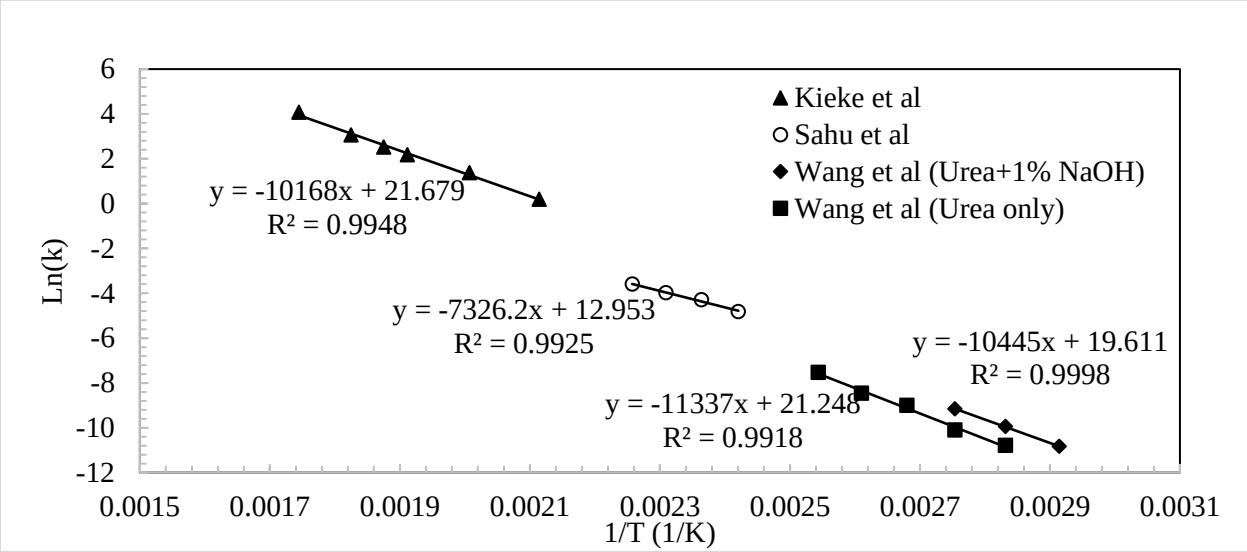

Figure 2-8 The reaction kinetics of urea hydrolysis at different temperatures, activation energy, and pre-exponential factor

Table 2-1 Activation energy and pre-exponential factor provided by authors [5,17,18,19]

Activation Energy and Pre-Exponential Factor			
Method	Activation energy, Ea (kJ/gmole)	Pre-exponential factor, A (1/min)	Temp Range, °C
Kieke, et al [4]	84.20	2.39E+09	200- 300
Sahu, et al [3]	73.64	2.89E+07	140 - 170
Urea only [1,2]	94.26	1.69E+09	70 - 120
Urea with 1%NaOH [1,2]	86.84	3.29E+08	70 -90

2.5. Oil Swelling

Oil swelling is one of the synergetic mechanisms in ICE. The partitioning of CO_2 causes oil swelling, and the amount of oil swelling depends on reservoir temperature, pressure, and oil composition. Oil swelling factor (S.F.) can be defined as the ratio of the volume of CO_2-oil mixture at reservoir conditions (pressure and temperature) to the volume of original oil at reservoir temperature and atmospheric pressure [20]. The swelling factor can be calculated as:

$$\text{Swelling factor (S.F.)} = \frac{V_{CO_2-oil}(P_R, T_R)}{V_{oil}(P_{atm}, T_R)} \quad \text{..... (2-18)}$$

Where V_{CO_2-oil} is the volume of oil and CO_2 mixture at reservoir temperature and pressure and V_{oil} is the volume of oil at reservoir temperature and atmospheric pressure. Oil swelling factor makes the oil saturation increase and which in turn also increases the oil relative permeability. Both volume swelling and viscosity reduction resulted from CO_2 dissolution in the oil will increase oil mobility. Additionally, the dissolution of CO_2 into oil also reduces the oil viscosity and mainly depends on the concentration of CO_2 in the oil and Figure 2-9 is a schematic of oil swelling processing.

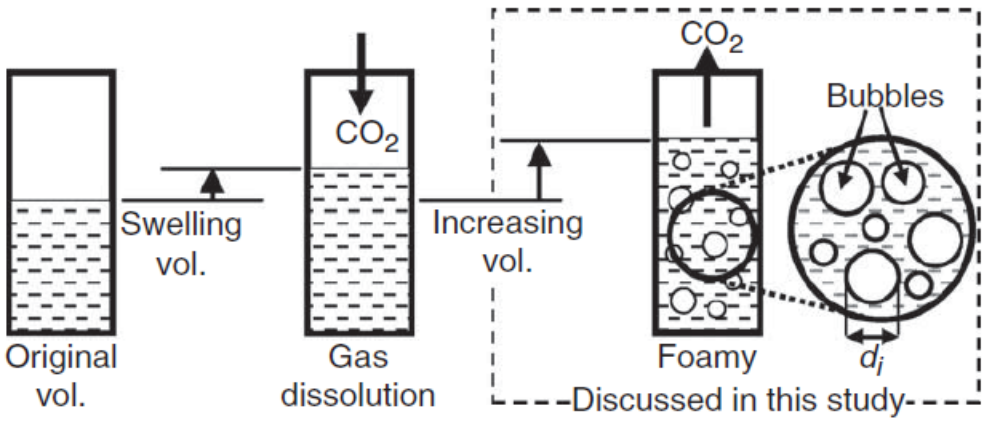

Figure 2-9 CO_2 partitioning into oil causing oil swelling and increase in oil volume [22]

If the reservoir pressure is below MMP, the dissolution of CO_2 into oil will be limited, and its solubility depends on pressure, temperature, and oil compositions. However, if the reservoir pressure is above MMP, the oil swelling factor almost linearly increases with increases in the CO_2 concentration in the oil. An equation of state (EOS) model was built to evaluate the swelling factor of octane under different concentrations of CO_2 and pressures. At a pressure of 3101 kPa (450 psi), CO_2 concentration is higher than 20% mole fraction, the swelling factor did not increase. It was partially dissolved the CO_2 and would work as an immiscible CO_2 EOR. Figure

2-10 shows the octane and CO_2 mixture swelling factor based on an EOS model. On top of this, the oil swelling factor is also affected by the reservoir temperature and oil types [22]. Oil swelling factor increases with decreasing temperature if the injection pressure is above MMP. It increases with decreasing oil viscosity at constant temperature and pressure above MMP. In other words, the lighter the oil, the higher will be the swelling factor. Figure 2-11 shows the relationships of oil swelling factor with pressure, temperature, oil viscosity, and oil volume [22].

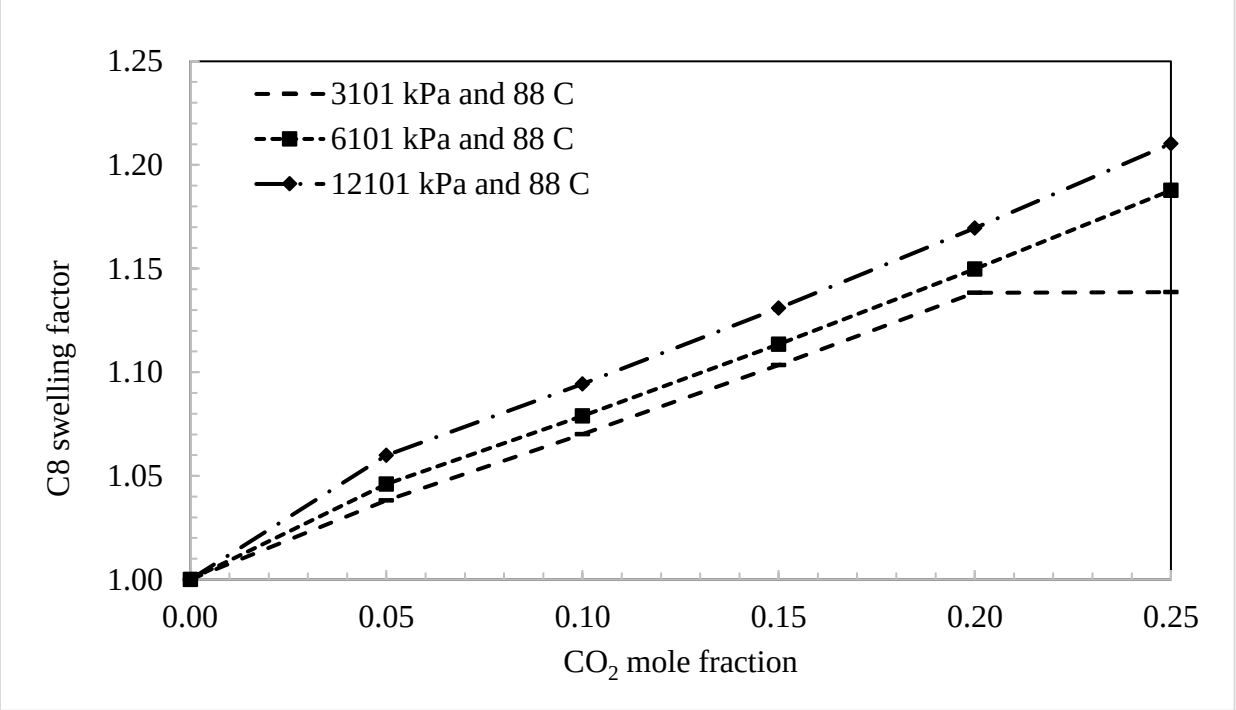

Figure 2-10 Octane and CO_2 mixture swelling factor at different pressures.

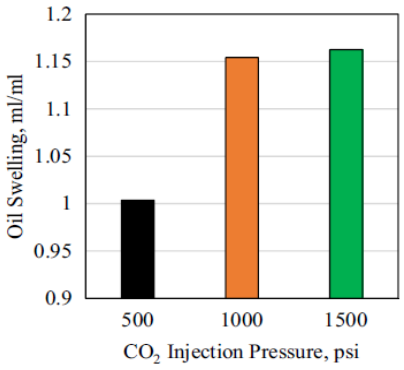

Fig. 2 Effect of CO_2 injection pressure on oil swelling at 40 °C using 1 ml of 460 cp oil

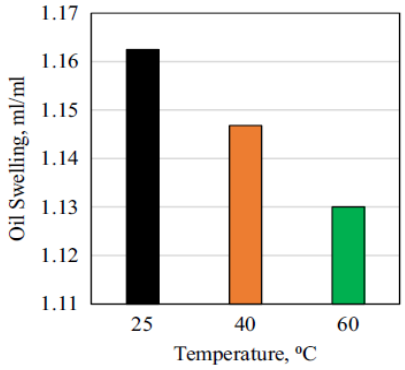

Fig. 3 Effect of temperature on oil swelling at 1500 psi using 1 ml of 470 cp oil

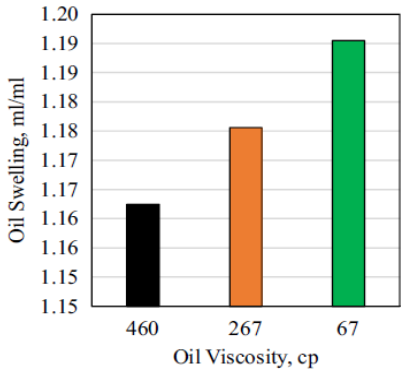

Fig. 4 Effect of oil viscosity on oil swelling at 1500 psi and 40 °C using 1 ml oil

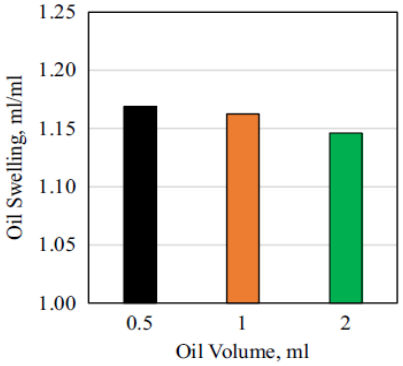

Fig. 5 Effect of oil volume on oil swelling at 1500 psi and 40 °C using 470 cp oil

Figure 2-11 Relationship between oil swelling and pressure, temperature, oil viscosity, and oil volume [18]

2.6. Oil and CO_2 Mixture Viscosity

Oil viscosity reduction in combination with oil swelling is another mechanism of ICE. Oil viscosity is reduced due to the partitioning of CO_2 into oil, making oil lighter and increasing its mobility in porous media. When an oil contact with CO_2 at high pressures, the non-Newtonian behavior of the crude oil was diminished and ultimately disappeared [23]. The primary parameter in the reduction of oil viscosity is the concentration of CO_2 in the oil. The CO_2 partitioning is the result of molecular diffusion [21]. There are different ways to measure and

calculate the crude oil and CO_2 mixture viscosity at different CO_2 concentrations. Researchers [20,21,22,23,24,25] measured the mixture viscosity with different experimental methods. Simon et al. [20] have reported that a two-step experimental procedure was used to measure the CO_2-Oil mixture viscosity. In the first step, the oil viscosity was measured using a viscometer at the atmospheric pressure and fixed temperature. In the second step, the mixture of oil and CO_2 was prepared, and the mixture viscosity and bubble-point pressure were measured at the same fixed temperature [20]. However, they did not report the properties of different crude oils used in the experimental procedure. Hu et al. [23] measured the mixture viscosity for heavy oil using a high-pressure circulation system and measured rheological properties of CO_2-oil mixture such as shear rate. They also reported phase behavior measurements of the CO_2-oil mixture. The provided the following correlations to calculate the mixture viscosity:

$$\ln(\eta_m) = -a_1 P + b_1 @\ p \leq p_{min} \quad \text{(2-19)}$$

$$\ln(\eta_m) = a_2 P + b_2 @\ p > p_{min} \quad \text{(2-20)}$$

Where η_m is the mixture viscosity (mPa.s), a_i and b_i (i=1,2) are the fitting parameters, and p_{min} is the pressure at which oil mixture viscosity reaches the minimum [23].

Barclay et al. [25] developed an empirical correlation to calculate CO_2 solubility in dead oil and oil viscosity reduction ratio due to CO_2 partition based on experimental data. This correlation was developed specifically for oils with 26° API or higher (specific gravity < 0.9). This correlation was based on reservoir pressure and temperature. The correlations for solubility of CO_2 in dead and oil viscosity reduction ratio are given below:

$$S = (0.36913 - 0.00106T)\ln(p) + (0.01280 - 0.00160T) \quad \text{(2-21)}$$

$$\frac{\mu_{oil-CO_2}}{\mu_{oil}} = 1 + (0.01113T - 1.78210)S \quad \text{..... (2-22)}$$

Where p is pressure (MPa) and T is the temperature (°C). The solubility (mole fraction) of CO_2 into dead oil under different CO_2 concentrations, pressures, and temperatures is shown in figure 2-12, and oil viscosity reduction ratio at different temperatures and CO_2-Oil solubility is shown in figure 2-13. They did not provide the solubility and oil viscosity ratio based on the mixing criteria of CO_2 into dead oil. Mixing can either be linear or non-linear. To consider the CO_2 mixing in the oil at different temperatures in this study, a linear mixing rule was used to compute the Oil-CO_2 mixture viscosities because CO_2 will be generated in-situ and controlled by reaction kinetics.

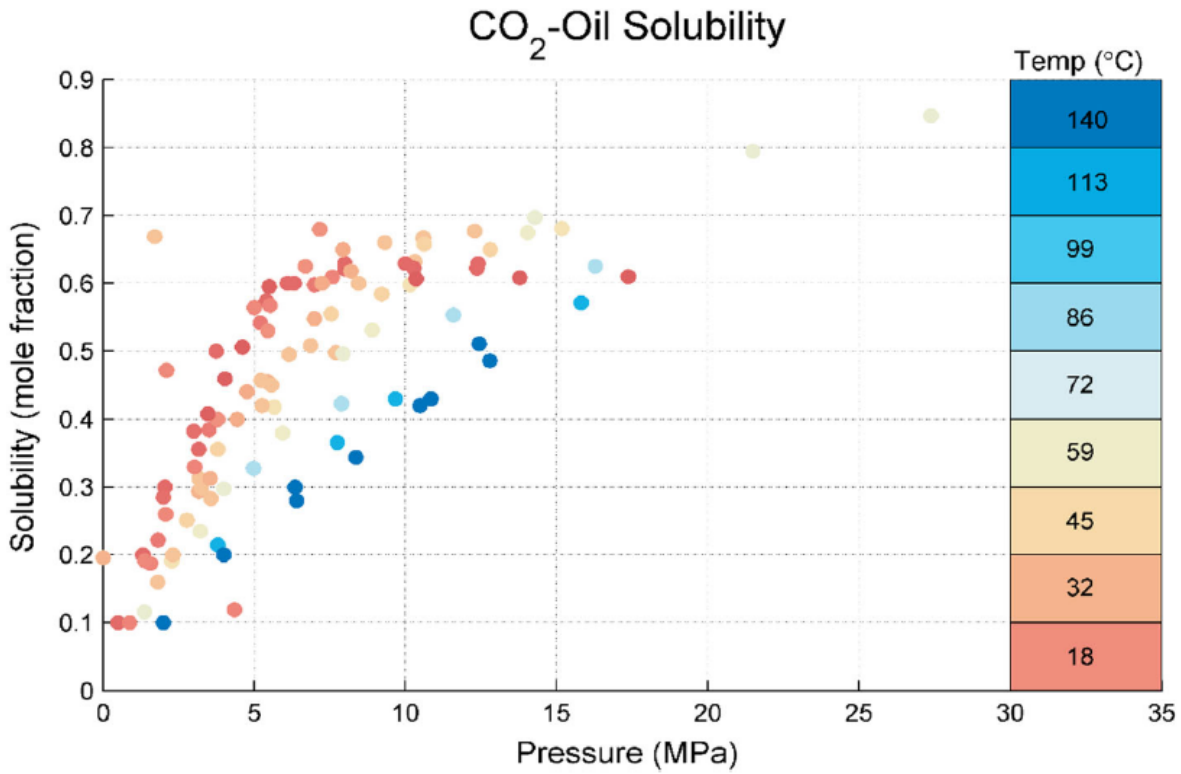

Figure 2-12 CO_2 solubility in the dead oil at different temperatures and pressures [25]

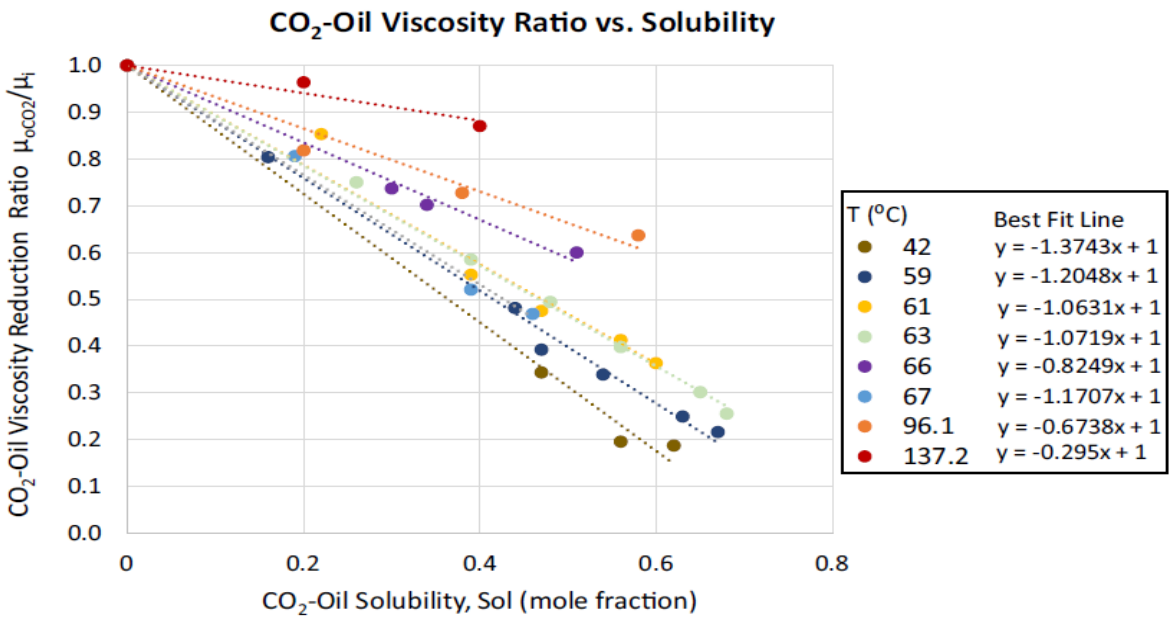

Figure 2-13 Oil viscosity reduction ratio at different temperatures and solubility concentration [25]

The oil and aqueous phase viscosities were calculated based on the following correlation described in CMG-STARS:

$$\text{Viscosity}_x = A_{visc}\exp^{(\frac{B_{visc}}{T_a})} \quad \text{..... (2-23)}$$

Where A_{visc} is the coefficient of the correlation for the temperature dependence of component viscosity in the liquid phases, it has a unit of viscosity (cp), B_{visc} is the temperature difference, and it has the unit of temperature (K), T_a is the absolute temperature (°R or K). The values A_{visc} and B_{visc} for different components is provided in Appendix-1. The oil-CO_2 mixture viscosity was calculated based on the linear mixing rule (Logarithmic Mixing Rule) as below:

$$\mu_o = (\mu_{CO_2})^x(\mu_{oi})^{1-x} \quad \text{.....(2-24)}$$

Where μ_{oi} is the original oil viscosity (cp), μ_{CO_2} is the CO_2 viscosity, x is the CO_2 mole fraction in the oil. Figure 2-14 shows the octane and CO_2 mixture viscosity under different CO_2 concentrations and temperatures.

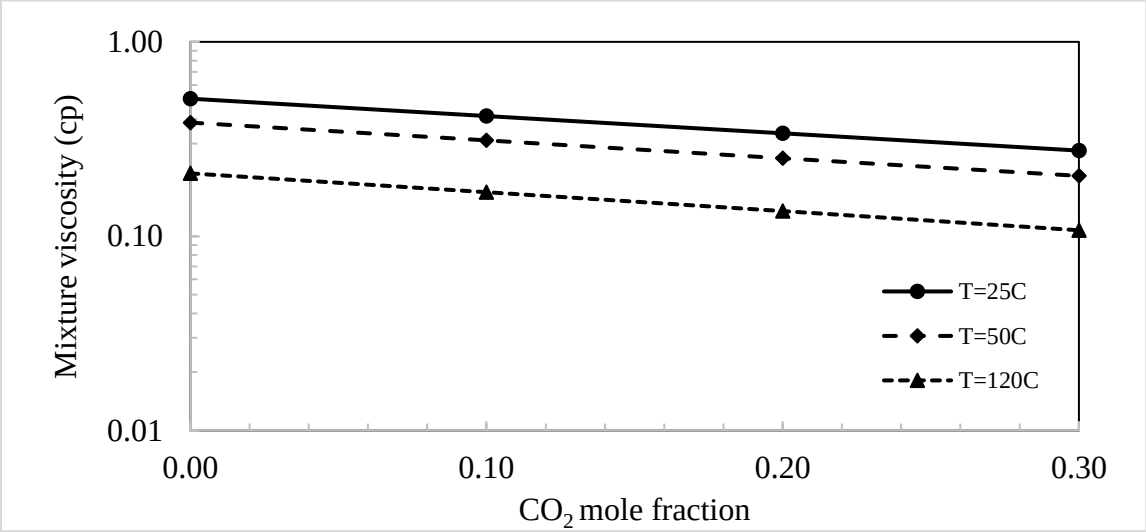

Chapter 3: Numerical Modeling of Urea Injection

This chapter explains the methodology used in the study to accomplish the objectives. This study is based on the objective to model the ICE mechanisms on a lab-scale and then upscale it to the field scale. In this study, CMG-STARS for modeling and simulation of fluid flow, and CMG-WinProp was used to study CO_2-Oil phase behavior. This research study was divided into different milestones based on objectives.

First, the reaction kinetics and Gibbs free energy of the urea hydrolysis reaction were studied. Secondly, a 1D numerical mechanistic model was built to evaluate the synergetic mechanisms, oil swelling, viscosity reduction, and wettability alteration involved in the ICE. Thirdly, the 1D mechanistic numerical model was used to history match the laboratory experiments performed for ICE by Wang [5]. The data provided by Wang [5] was used to build the 1D mechanistic numerical models. After history matching and analyzing the uncertainties in history matching, the 1D mechanistic numerical model was upscaled to a 3D quarter 5-spot ICE model. The sensitivity analysis was performed on reservoir temperature, urea concentration, injection rate, and shut-in/no shut-in. The optimized scenario was selected based on the sensitivity analysis and incremental oil recovery.

3.1. Reaction Kinetics and Gibbs free energy

The chapter 2 literature review explained that reaction kinetics provides the reaction rates of the urea hydrolysis reaction. Different researchers [5, 17, 18, 19] have investigated the reaction equilibrium, reaction order, and reaction kinetics of the urea hydrolysis reaction. The reaction rates are highly affected by temperature, activation energy, and the pre-exponential factor of the reaction. Wang et al. [5,17] reported reaction rates of urea hydrolysis for temperatures between

70°C and 120°C. The reaction rates of urea hydrolysis at different temperatures are provided in Table 3-1:

Table 3-1 Reaction rates of urea hydrolysis reported by Wang et al. [5,17]

Urea Only			
Temp (°C)	k (1/min)	ln(k)	1/T (1/K)
70	1.41E-06	-13.47	0.0029
80	2.06E-05	-10.79	0.0028
90	4.09E-05	-10.11	0.0028
100	1.22E-04	-9.01	0.0027
110	2.12E-04	-8.46	0.0026
120	5.37E-04	-7.53	0.0025

Wang et al [5,18] added 1 wt.% NaOH in the urea solution and measured the reaction rates of the reaction as shown in Table 3-2:

Table 3-2 Reaction rates of urea hydrolysis with 1 wt. % NaOH reported by Wang et al. [5,17]

Urea with 1% NaOH			
Temp (°C)	k (1/min)	ln(k)	1/T, 1/K
70	1.97E-05	-10.83	0.0029
80	4.76E-05	-9.95	0.0028
90	1.05E-04	-9.16	0.0028

Adding NaOH to the urea solution increases the reaction rates for low temperatures. Therefore, in the following numerical simulation study, temperatures higher than 100°C were used to examine the decomposition of urea into ammonia and carbon dioxide. Similarly, Sahu et al. [17] and Kieke et al. [19] also measured the reaction rates of urea hydrolysis at different temperatures, and their results are summarized in Figure 2-8. Additionally, the researchers [5,17,18,19] also estimated activation energy and pre-exponential factor of the urea reaction based on measured reaction rates. The activation energy and pre- exponential factor by different authors are provided in Table 2-1.

Based on a wide range of activation energy and pre-exponential factor, reaction rates using different activation energies and pre-exponential factors were calculated and the Arrhenius model at 120°C temperature and Arrhenius equation is given in 2-17. The reaction rates for different activation energies and temperatures are shown in Figure 3-1:

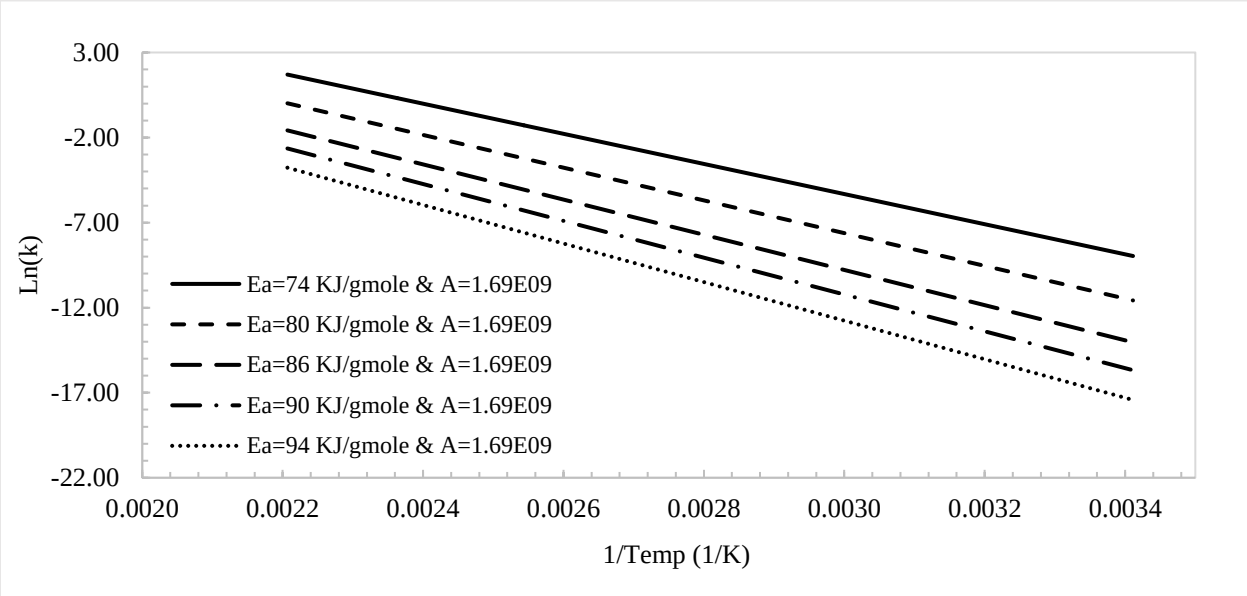

Figure 3-1 Reaction rates of urea hydrolysis reaction at different activation energies and temperatures

Figure 3-1 shows that the lower the activation energy, the higher is the reaction rate. In the numerical model, activation energy and pre-exponential factor were modified to match CO_2 moles from laboratory experiments. In this simulation study, it was noticed that using reaction kinetics reported in the above literature could not produce enough amount of CO_2 to match the reported oil recovery by Wang et al. [18]. The hypothesis of modifying the laboratory-determined parameters is that these parameters are different in porous media versus the laboratory bulk phase behavior under the same temperature. Additionally, the laboratory tests did not consider the pressure effect on these parameters. Therefore, these parameters were modified to obtain the CO_2 moles at a specific urea concentration.

In addition to reaction kinetics, Gibbs free energy of urea hydrolysis reaction was computed at different temperatures. Gibbs free energy measures the potential energy of a chemical reaction. It can be used to predict the properties of chemical energy [27]. Gibbs free energy can be computed as:

$$G = H - TS \qquad \text{..... (3-1)}$$

Where G is Gibbs free energy (kJ/mol), H is the heat energy (kJ/mol), T is the system temperature (Kelvin), and S is the entropy of the system (kJ/mol·K). A change in the free energy of the reaction can be measured as:

$$\Delta G = G_{products} - G_{reactant} = H_{products} - H_{reactants} - T(S_{products} - S_{reactants}) \text{.. (3-2)}$$

$$\Delta G = \Delta H - T\Delta S \quad \text{..... (3-3)}$$

Where G, H, and S, are Gibbs free energy, heat energy, and entropy of reactants and products, respectively. ΔG, ΔH, and ΔS are the change in the free energy, heat energy, and entropy of the reaction, respectively. If the free energy of reactants is higher than the free energy of the products, $G_{reactants} > G_{products}$, the reaction will be spontaneous. A spontaneous reaction always releases energy. Therefore, the ΔG must be negative. If the ΔG is positive, the reaction will be non-spontaneous. Computation of the change in the free energy of the reaction at different temperatures can be used to predict the reaction direction. The data of standard enthalpy and entropy of urea hydrolysis reaction is provided in Table 3-3 [26,27]. Figure 3-2 shows Gibbs free energy of urea hydrolysis at different temperatures:

Table 3-3 Standard Enthalpy and Entropy of Urea hydrolysis reaction (14.7 psi and 25°C)

Standard Enthalpy and Entropy of Urea Hydrolysis Reaction		
Component	Enthalpy (kJ/mol)	Entropy (kJ/mol.K)
Urea	-319.20	0.1738
Water	-285.90	0.0700
CO_2	-393.50	0.2135
NH_3	-46.19	0.1925

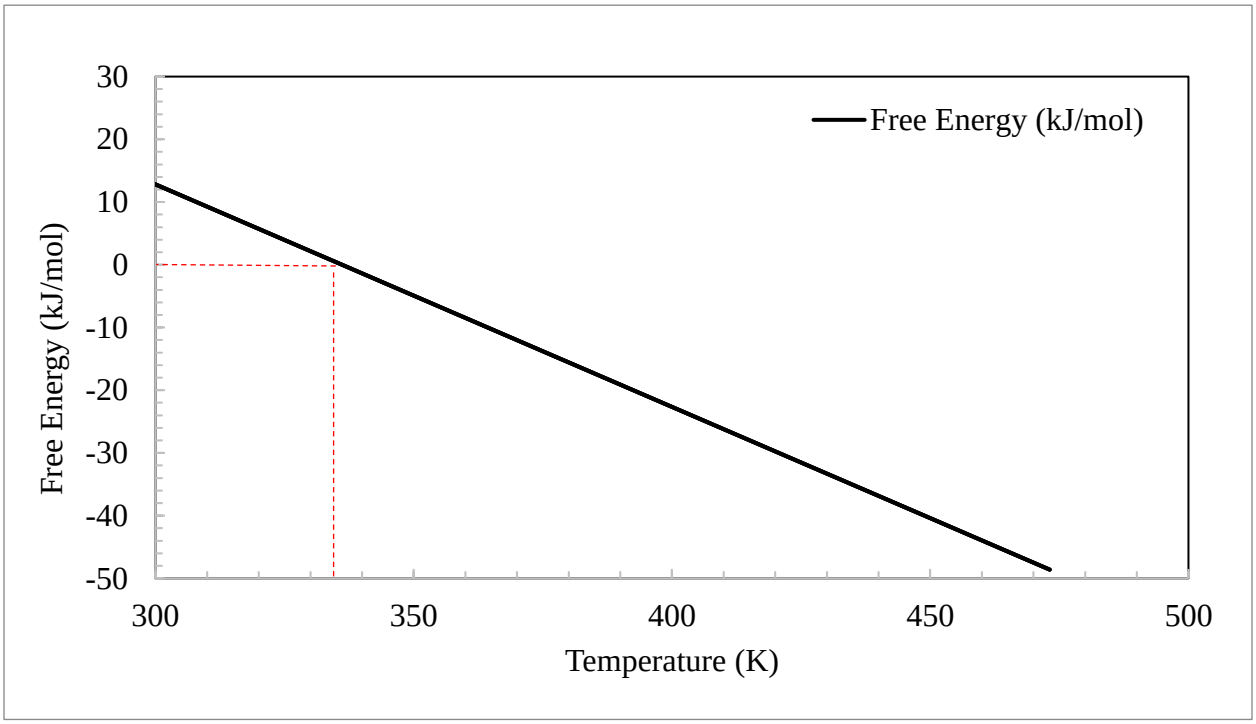

Figure 3-2 Gibbs free energy of urea hydrolysis reaction.

Figure 3-2 shows that Gibbs free energy becomes negative above the 340K (~70°C) temperature. The urea hydrolysis reaction becomes spontaneous when the temperature is above 70°C temperature. Hence, to apply urea as a CO_2 generating agent, one of the critical design parameters is that the reservoir temperature must be higher than 70 °C. The reaction rate can only be increased if a catalyst is added to the urea solution, such as sodium hydroxide.

3.2. 1D Mechanistic Numerical Model

Based on the analysis of reaction kinetics and reaction rates, a 1D mechanistic numerical model was built to simulate and match the laboratory experiments. A sensitivity analysis was performed to select the best grid size without any convergence problems. From this exercise, the model uses 100 grid blocks in the flow direction. The 1D mechanistic numerical model was based on 1 injector and 1 producer wells. The grid and input data of the 1D mechanistic numerical model is provided in Table 3-4:

Table 3-4 1D mechanistic numerical model grid and rock properties

Grid and Rock Properties	
Property	Value
Grid Dimensions (x*y*z)	100*1*1
X-direction block size (cm)	0.31
Y-direction block size (cm)	2.00
Porosity (frac)	0.10
Permeability (x, y and z)	100 mD
Water saturation	0.50
Thickness (cm)	2.00

The 1D mechanistic numerical model is shown in Figure 3-3. Octane (C_8H_{18}) was used as the oleic phase in the model. An EOS model was built to calculate the phase behavior, molar volumes, and fluid properties of octane at different pressures and temperatures.

The urea hydrolysis reaction, reaction stoichiometry, and kinetics were incorporated into the model. The properties of urea, ammonia, carbon dioxide, water, and octane are provided in Table 3-5. The critical properties and densities of all the components other than octane were taken from the National Institute of Standards and Technology (NIST) [28].

Table 3-5 Properties of Components in 1D Mechanistic Numerical Model

Properties of Components				
Component	Critical Pressure (psi)	Critical Temperature (°F)	Molecular Weight (lb/lbmole)	Density (lb/ft^3)
Urea	688.96	1122.00	60	83.03
CO_2	1069.80	87.89	44	49.19
Water	3197.50	705.10	18	62.40
NH_3	1638.93	270.05	17	38.55
C_8H_{18}	427.95	567.23	107	42.08

The viscosity of the octane and mixture viscosity of octane and CO_2 was estimated using viscosity correlation in CMG-STARS. A linear correlation aforementioned was used because it has better control on temperature and concentration of CO_2 in the oleic phase.

The viscosity of octane at different temperatures is given in Table 3-6. The estimated viscosity of octane was incorporated in the numerical model.

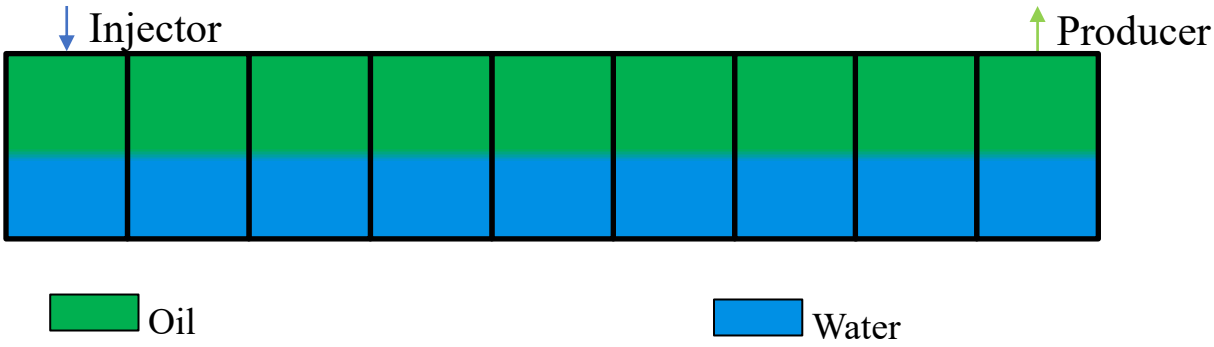

Figure 3-3 1D mechanistic numerical model

Table 3-6 Octane Viscosity estimated using CMG-STARS viscosity correlation.

Octane Viscosity	
Ta (°C)	Viscosity (cp)
120	0.21
88	0.27
60	0.35
25	0.51

Similarly, the viscosity of CO_2 and water were estimated and incorporated into the model. Likewise, the mixture viscosity of octane and CO_2 was estimated using linear (Logarithmic) mixing rule viscosity correlation used by CMG-STARS (equation 2-24).

Figure 3-4 shows the octane and CO_2 mixture viscosity under different CO_2 concentrations and temperatures. After running the numerical model, the mixture viscosities were examined and were matching with the estimated viscosity.

In addition to the viscosity of octane and mixture viscosity of octane and CO_2, the oil swelling factor was estimated using a two-phase flash EOS model. The oil swelling factor is shown in Figures 3-5 under different CO_2 concentrations and pressures. It can be observed that pressure above 3101 kPa, CO_2 is miscible in octane, and swelling factor is increasing linearly with an increase in CO_2 concentration in the octane. Hence, this pressure is believed to be minimum

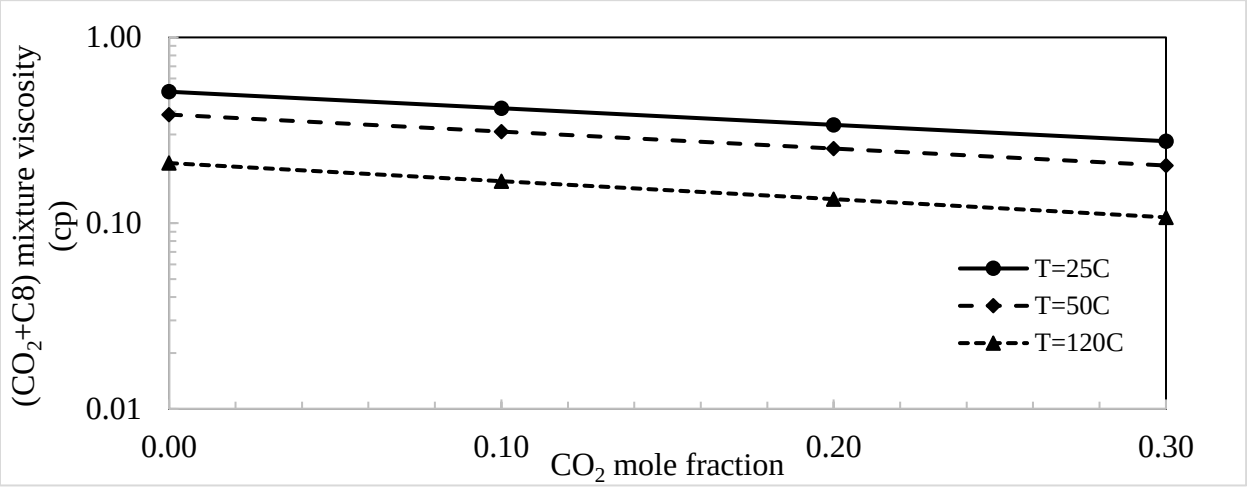

Figure 3-4 Mixture viscosity of octane and CO_2 under different CO_2 concentrations and temperatures

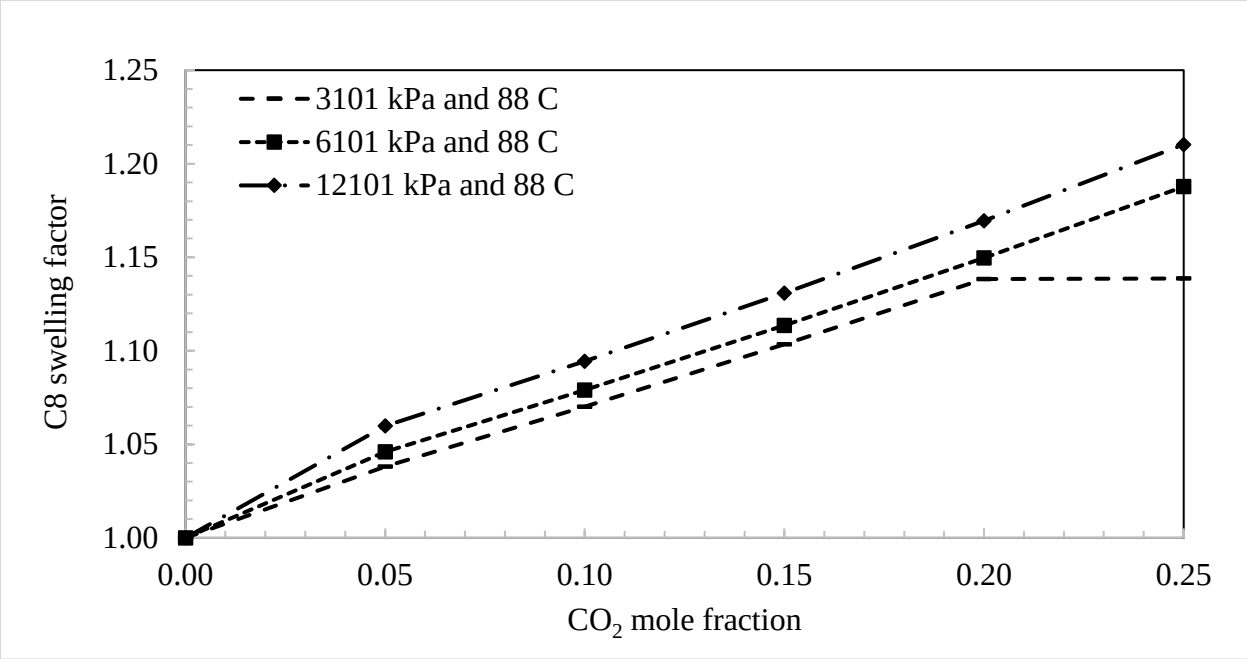

Figure 3-5 Oil swelling factor under different CO_2 concentrations and pressures

miscibility pressure (MMP). Therefore, based on this observation, the injection pressure was kept well above 3101 kPa in the mechanistic model. The relative permeability of the oil and water was estimated using Corey two-phase relative permeability correlation.

Additionally, the ammonia alkali (in-situ surfactant) mechanism was incorporated in the numerical model through CMG-STARS built-in process workflow of alkali/surfactant/polymer injection. The ammonia concentration was estimated based on reaction stoichiometry, and the built-in process workflow calculated interfacial tension (IFT) of 50 dynes/cm. Since there is no petroleum acid in the octane and there was no direct measurement of octane/water IFT available, the IFT data used in the model was based on Karen Li's [14] measurement dodecane/water IFT at different urea concentrations at 25°C and 1 atm. The earlier discussion shows that urea hydrolysis reaction becomes spontaneous at temperatures higher than 70°C. Li [14] performed IFT measurements based on different urea concentrations for dodecane and middle eastern oil and are shown in Figure 3-6. This reduction of IFT might not be the result of ammonia and CO_2 partitioning because urea hydrolysis reaction has not started decomposing into ammonia and CO_2

to have the synergetic mechanism of ammonia alkali and IFT reduction at 25°C and 1 atm. Therefore, IFT measurements performed by Li [14] were not due to ammonia alkali.

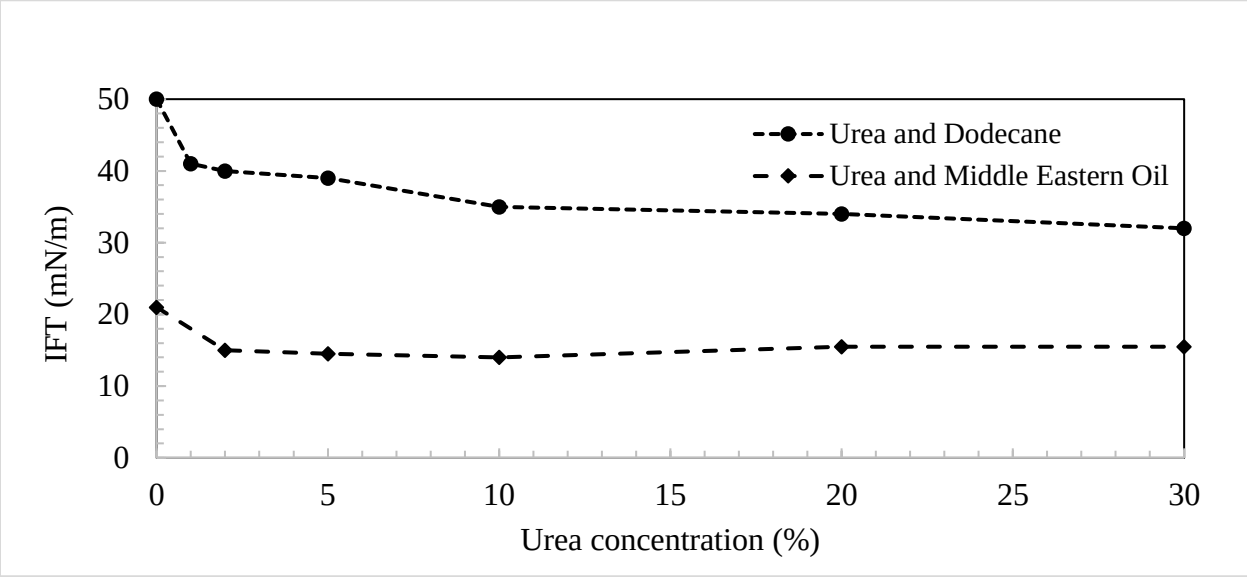

Figure 3-6 IFT measurements under different urea concentration for dodecane and middle eastern oil [14]

Yuan [30] used urea as a hydrotrope to solubilize the hydrophobic compounds in an aqueous solution [30]. It works as a salting process and increases the charge of the solute molecule. Similarly, the hydrotropes have hydrophobic and hydrophilic parts like surfactants. However, urea as a hydrotrope works as alcohol at lower temperatures [30]. Due to the hydrogen-hydrogen bond with carbon and a carboxylic acid, it works as a surfactant at lower temperatures and reduces interfacial tension without undergoing urea hydrolysis reaction [30]. The model was run after incorporating model components, urea hydrolysis reaction, stoichiometry, kinetics, and viscosity of components. A sensitivity analysis was performed to optimize the reaction rate to produce desired CO_2 moles based on urea concentration. The results and observations based on the 1D mechanistic numerical model will be discussed in Chapter 4 Results and Observations.

3.3. 1D Laboratory Numerical Models

The second objective was to validate the synergetic mechanisms based on laboratory experiments performed by Wang [5,18]. Wang [5,18] conducted 11 laboratory experiments based on different oil compositions and operating strategies to evaluate the incremental oil recovery by ICE. The model validation is to history match the oil saturation profiles as observed in the lab with the same injection scheme. The purpose of building 1D lab mechanistic numerical models was to match the laboratory experiments to chemical reaction parameter and displacement relative permeabilities, history match the oil saturation vs pore volume injected of ammonium carbamate and brine, and validate the synergetic mechanisms of ICE. Three laboratory experiments were picked based on different oil compositions, i.e., dodecane, Earlsboro Oil, and DeepStar Oil. The data of three laboratory experiments is provided in Table 3-7.

Table 3-7 ICE Laboratory experiment data used for lab mechanistic numerical models [5,18]

ICE laboratory experiments selected for History Matching									
Test	Oil	φ (%)	K* (md)	Sor after waterflooding (%)	PV (cc)	Temp (°C)	Inj. Pres (psi)	Flow rate (cc/min)	Urea concentration (wt.%)
Test-1	Dodecane	34.3	4006.4	22.6	18.934	120	1500	0.03	35
Test-2	Earlsboro	33.9	3929.0	50.0	18.645	120	1500	0.03	35
Test-3	DeepStar	34.0	3939.2	28.9	18.700	120	1500	0.03	35

* *permeability in x, y, and z-direction*

The length of cores in the laboratory experiments was 6 inches and the inside diameter of the cores was 0.834 inches [8]. Based on the length and diameter of the cores in the laboratory experiments, the 1D lab mechanistic models were built with 51 grid blocks in the x-direction. The EOS models were built based on oil compositions used by Wang [5,18] in their lab experiments. The oil compositions of Earlsboro and DeepStar oils are provided in Figures 3-7

and 3-8 [5,18]. The original oil composition of Earlsboro oil sample was available, whereas, for DeepStar, oil composition after brine flooding was available [5]. The EOS models of Earlsboro and DeepStar oils were lumped into one component and incorporated in the 1D lab mechanistic models. The lumped components were named Earlsboro oil for Earlsboro and DeepStar oil for DeepStar. The critical properties of dodecane, Earlsboro oil, and DeepStar oil are provided in Table 3-8.

Table 3-8 Critical properties of oleic phase components in Lab Mechanistic Numerical Models

Properties of Components in 1D Lab Mechanistic Numerical Models				
Component	Critical Pressure (psi)	Critical Temperature (F)	Molecular Weight (lb/lbmole)	Density (lb/ft3)
Dodecane	317.87	735.35	161	44.52
Earlsboro oil	329.41	723.23	162	46.55
DeepStar oil	307.18	764.15	179	46.62

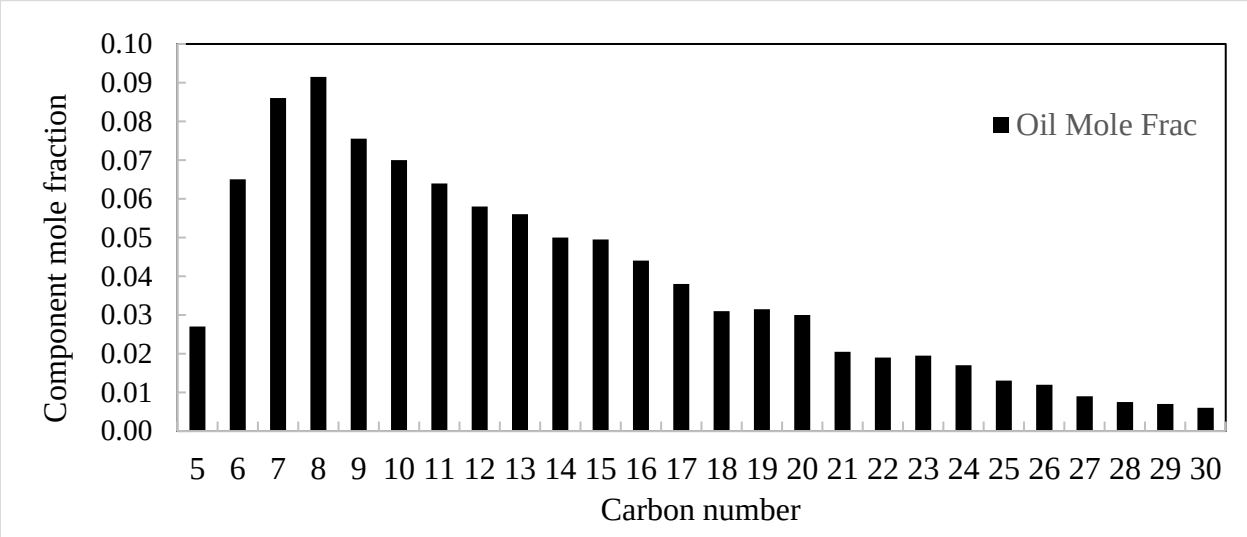

Figure 3-7 Earlsboro original dead oil composition [5]

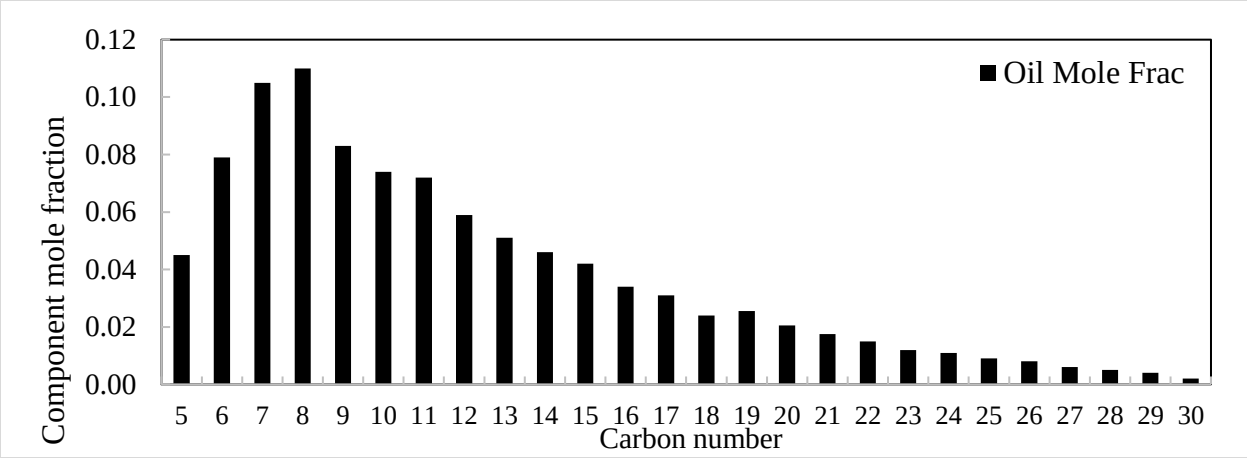

Figure 3-8 DeepStar original dead oil composition after brine flooding [5]

The physical properties of dodecane, Earlsboro, and DeepStar oil samples at atmospheric pressure and room temperature (25°C) used in laboratory experiments by Wang [5] are provided in Table 3-9.

Table 3-9 Physical properties of Dodecane, Earlsboro, and DeepStar oil samples at atmospheric pressure and 25°C temperature [5]

API and Viscosity of oil samples		
	˚API	Viscosity (cp)
Dodecane	57.30	1.340
Earlsboro	40.00	4.60
DeepStar	27.00	22.00

Based on available viscosity data of dodecane, Earlsboro, and DeepStar oil samples, the coefficients of CMG-STARS viscosity correlations (equation 3-6), A_{visc} and B_{visc} were modified to match the viscosities of oil samples at 25°C and extrapolated to different temperatures for 1D lab mechanistic models. The matched coefficients of CMG-STARS viscosity correlation and estimated viscosities of dodecane, Earlsboro oil, and DeepStar oil at different temperatures are provided in Tables 3-10 and Table 3-11. Similarly, the mixture viscosities of CO_2 and dodecane, Earlsboro oil, and DeepStar oil were calculated using Equation 3-7 and are shown in Figures 3-9, 3-10, and 3-11, respectively.

Table 3-10 CMG-STARS viscosity correlation matched coefficients at 25°C

Viscosity Correlation Matched Coefficients			
Oleic Component	Matched A_{visc} (cp)	Matched B_{visc} (K)	Matched Viscosity at 25°C
Dodecane	0.0104	1446.80	1.34
Earlsboro oil	0.0095	1842.00	4.60
DeepStar oil	0.0064	2424.61	22.00

Table 3-11 Viscosities of dodecane, Earlsboro oil, and DeepStar oil based on different temperatures.

Viscosities of Dodecane, Earlsboro oil, and DeepStar oil based on CMG-STARS Viscosity Correlation						
Oleic Component	Viscosity (cp)					
	25°C	50°C	80°C	100°C	120°C	150°C
Dodecane	1.34	0.92	0.63	0.50	0.41	0.32
Earlsboro oil	4.60	2.85	1.76	1.33	1.03	0.74
DeepStar oil	22.00	11.72	6.19	4.28	3.08	1.99

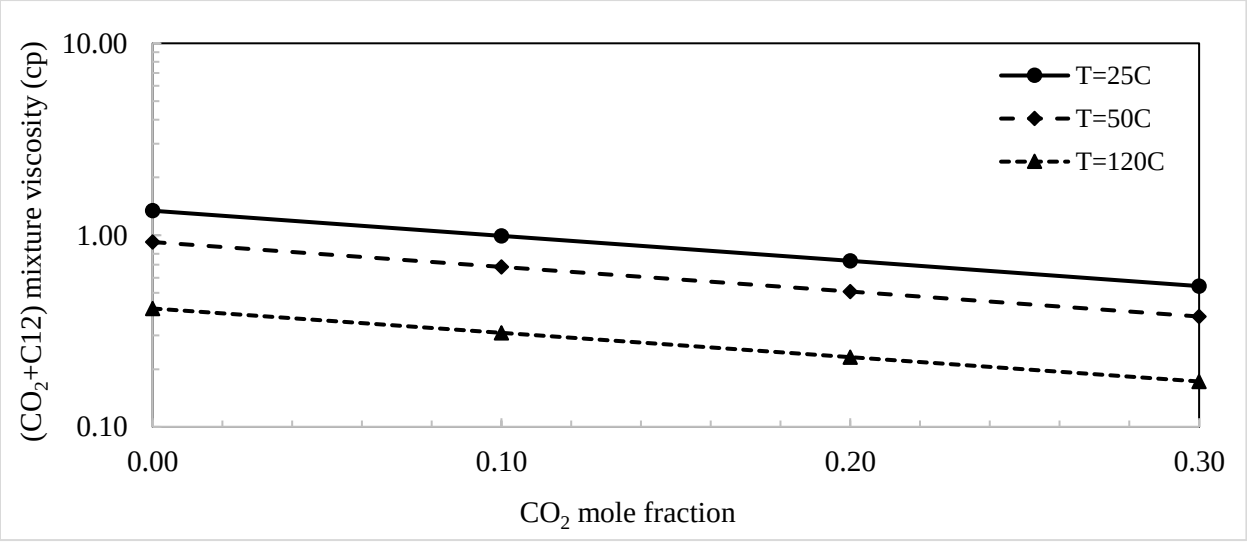

Figure 3-9 Dodecane and CO_2 mixture viscosity under different CO_2 concentrations and temperatures

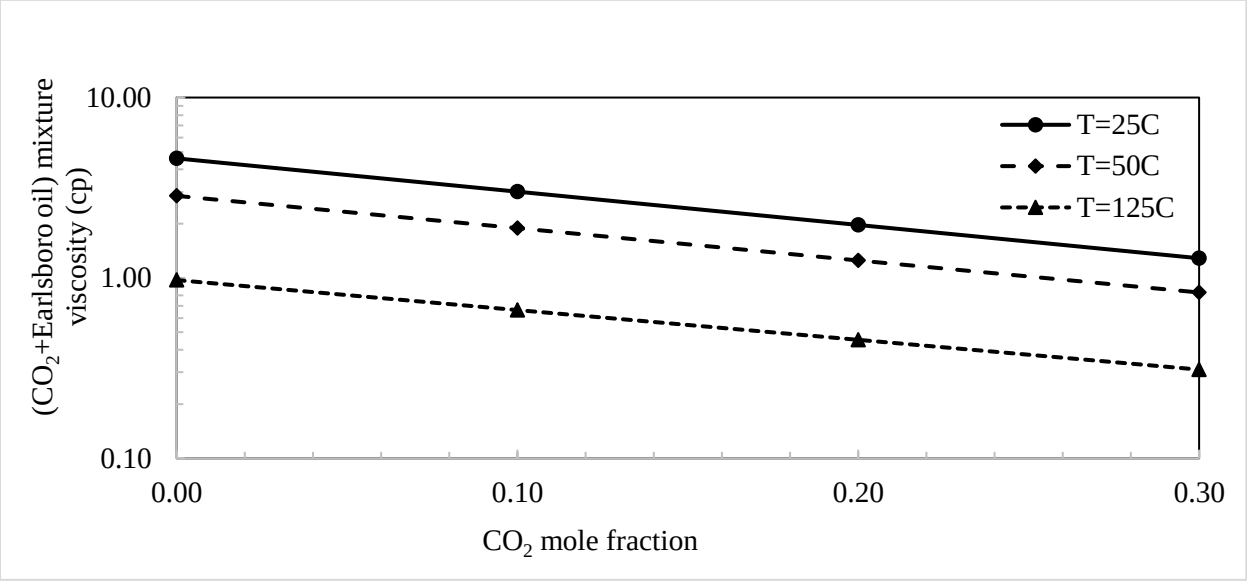

Figure 3-10 Earlsboro oil and CO_2 mixture viscosity under different CO_2 concentrations and temperatures

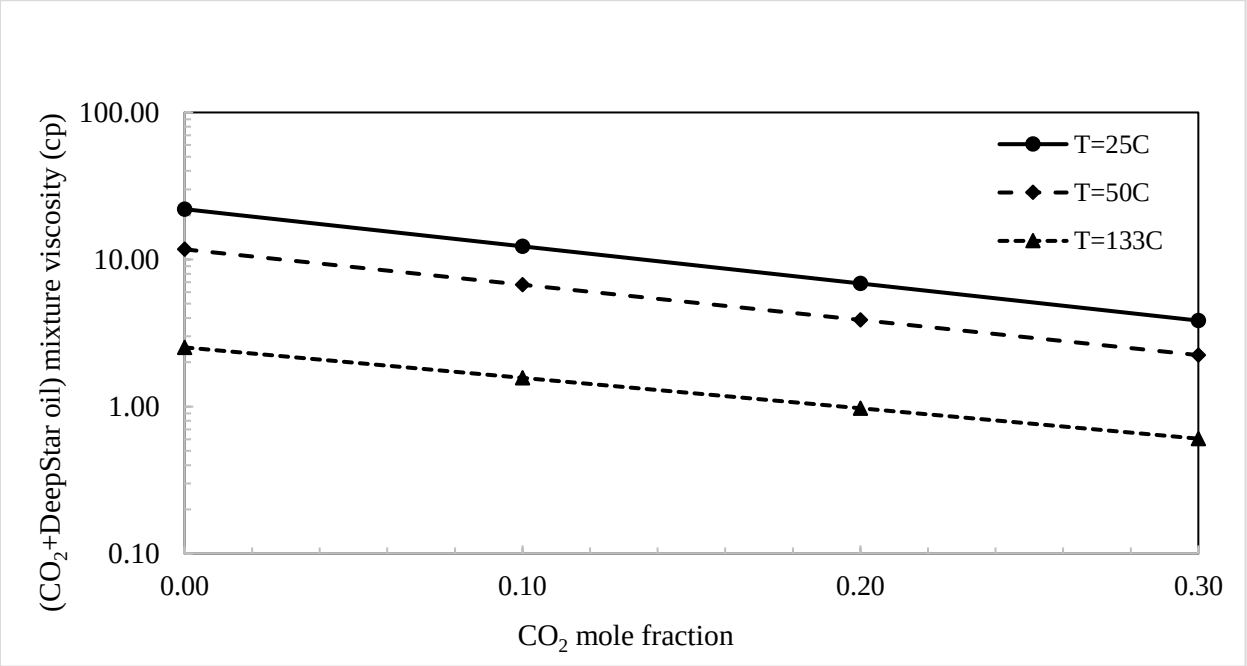

Figure 3-11 DeepStar oil and CO_2 mixture viscosity under different CO_2 concentrations and temperatures

Wang [5] used 35 wt.% urea concentration in Test-1, 2, and 3, provided in Table 3-7. The urea injection mole fraction was estimated based on the density of urea and water and urea concentrations. The water density was calculated using EOS to be 788 kg/m^3 (49.19 lb/ft^3) at 120°C. The molar calculations of 35 wt.% urea concentration and 100 gm solution at 120°C are provided in Table 3-12.

Table 3-12 The molar calculations for urea injection at 120°C

Molar Calculations of Urea at 120°C				
Component	Mass concentration (frac)	Mass (kg)	Moles	Mole fraction
Urea	0.35	0.035	0.58	0.14
Water	0.65	0.065	3.61	0.86

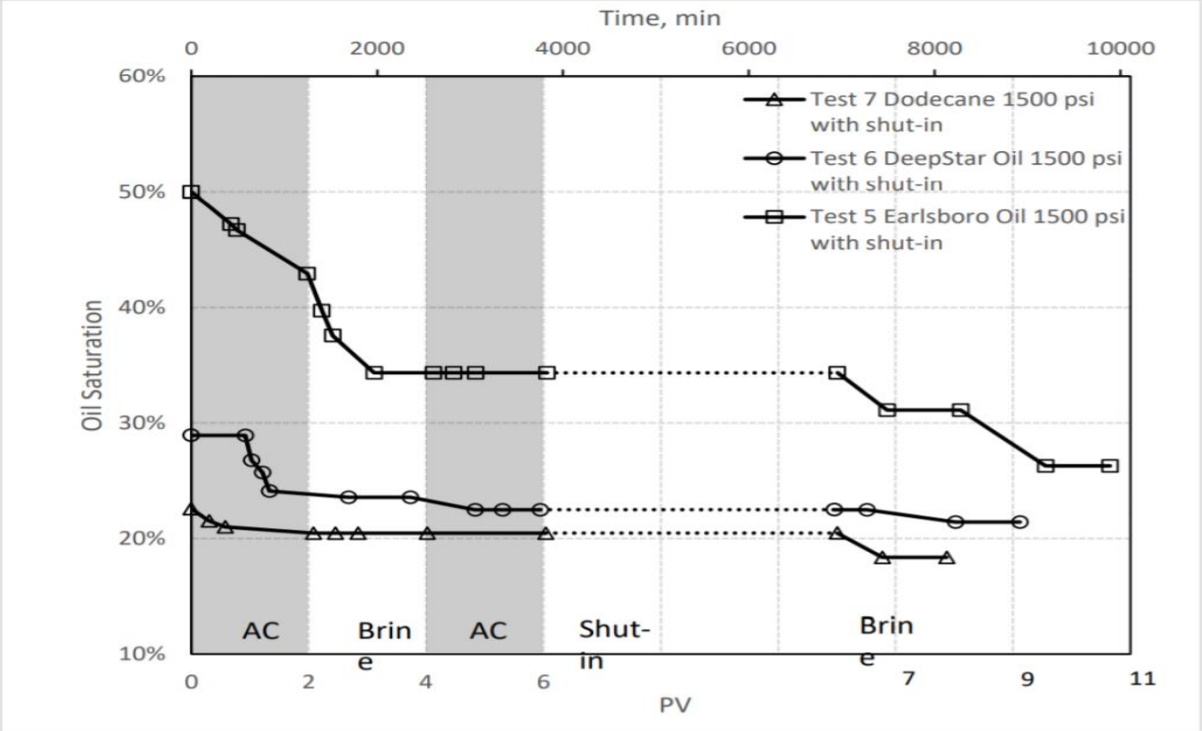

Figure 3-12 Laboratory measured oil saturation and pore volume injected of ammonium carbamate and brine for different oil compositions and tests [5]

Based on the molar calculation at 35 wt. % urea concentration, 0.14 mole fraction of urea were used for injection in three 1D lab mechanistic numerical models. Wang [5] performed laboratory

experiments based on different injection and shut-in strategies. The laboratory measured oil saturation versus pore volume of urea and brine injected during the ICE laboratory experiments by Wang [8] is shown in Figure 3-12. Figure 3-12 shows that initially two pore volumes (PV) of ammonium carbamate solution were injected, followed by two PV of brine, followed by two PV of ammonium carbamate, followed by a shut-in of injection and production for almost 5 PV, and followed by 2-5 PV of brine in Test-1 (Test-7 in Figure 3-12), 2 (Test-5 in Figure 3-12), and 3 (Test-6 in Figure 3-12). Therefore, similar operating strategies of ammonium carbamate and brine were incorporated in the 1D lab mechanistic numerical models for history matching and ICE synergetic mechanisms validation.

The molar calculations were performed for quality checking purposes, and CO_2 moles were back-calculated based on multiple injection cycles of ammonium carbamate, followed by a shut-in in the laboratory experiments. The CO_2 moles produced during the urea hydrolysis reaction in the 1D lab mechanistic numerical models matched the molar calculations. The molar calculations at different urea mole fractions are provided in Table 3-13. Additionally, similar reaction kinetics were used in the lab numerical model in the 1D mechanistic numerical model.

The relative permeability of oil and water was estimated using a two-phase Corey relative permeability correlation because there was no relative permeability measurement available for the laboratory experiments. The relative permeability of water and end-point saturations were modified to history match the measured oil saturation at different pore volumes.

Table 3-13 Urea molar calculations based on operating strategies under different urea mole fractions.

Urea molar calculations under different urea mole fractions				
Urea mole fraction	Urea Solution injection rate (cc/min)	Urea mass (kg/min)	Urea (moles/min)	Total Urea (moles) Including Shut-in
6%	0.0018	2.39E-06	3.99E-05	**0.23**
14%	0.0042	5.59E-06	9.31E-05	**0.53**
21%	0.0063	8.38E-06	1.40E-04	**0.79**
28%	0.0084	1.12E-05	1.86E-04	**1.06**
35%	0.0105	1.40E-05	2.33E-04	**1.32**

Since the molar ratio of urea and CO_2 is 1:1 (the stoichiometric equation is given in 1-1), therefore, the urea moles produced would be considered CO_2 moles produced given sufficient reaction time at the set temperature.

Additionally, the oil swelling factor was calculated for dodecane, Earlsboro oil, and DeepStar oil based on EOS. The oil swelling factor of dodecane, Earlsboro oil, and DeepStar oil is shown in Figures 3-13, 3-14, and 3-15. It can be observed that in the two cases with pressure above 3101 kPa (450 psi) pressure, CO_2 is miscible in dodecane, and the swelling factor is increasing linearly concerning increasing in CO_2 concentration in dodecane. This shows that when pressure is 3101 kPa and 15% CO_2 mole fraction, the system is not in miscibility. Similar behavior was observed for Earlsboro oil and DeepStar oil. Additionally, the IFT measurements under different urea concentrations and oil compositions were performed by Li [14]. The IFT measurements of dodecane under different urea concentrations at 25°C and 1 atm are shown in Figure 3-16.

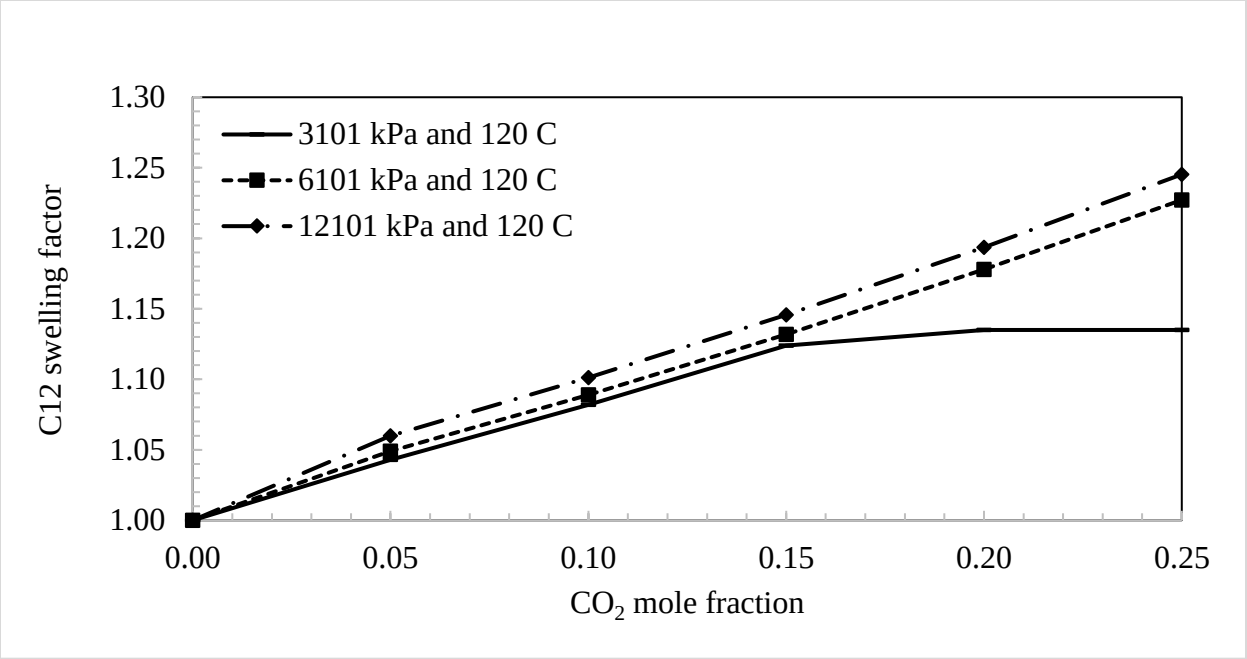

Figure 3-13 Dodecane swelling factor under different CO_2 concentrations and pressures.

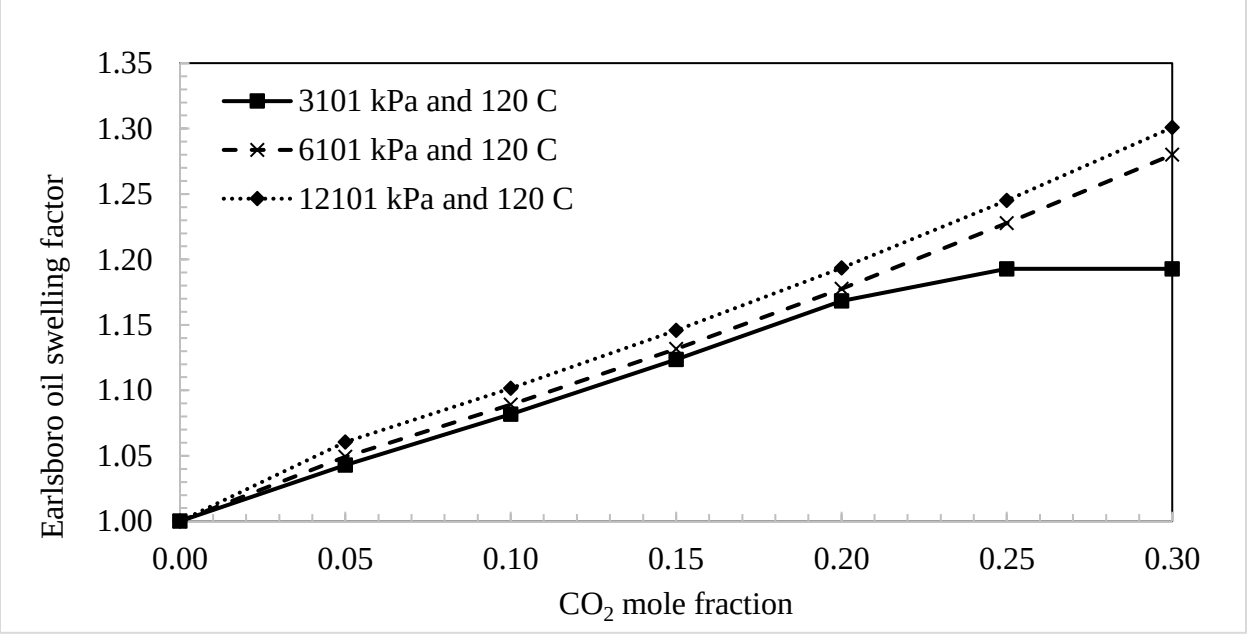

Figure 3-14 Earlsboro oil swelling factor under different CO_2 concentrations and pressures.

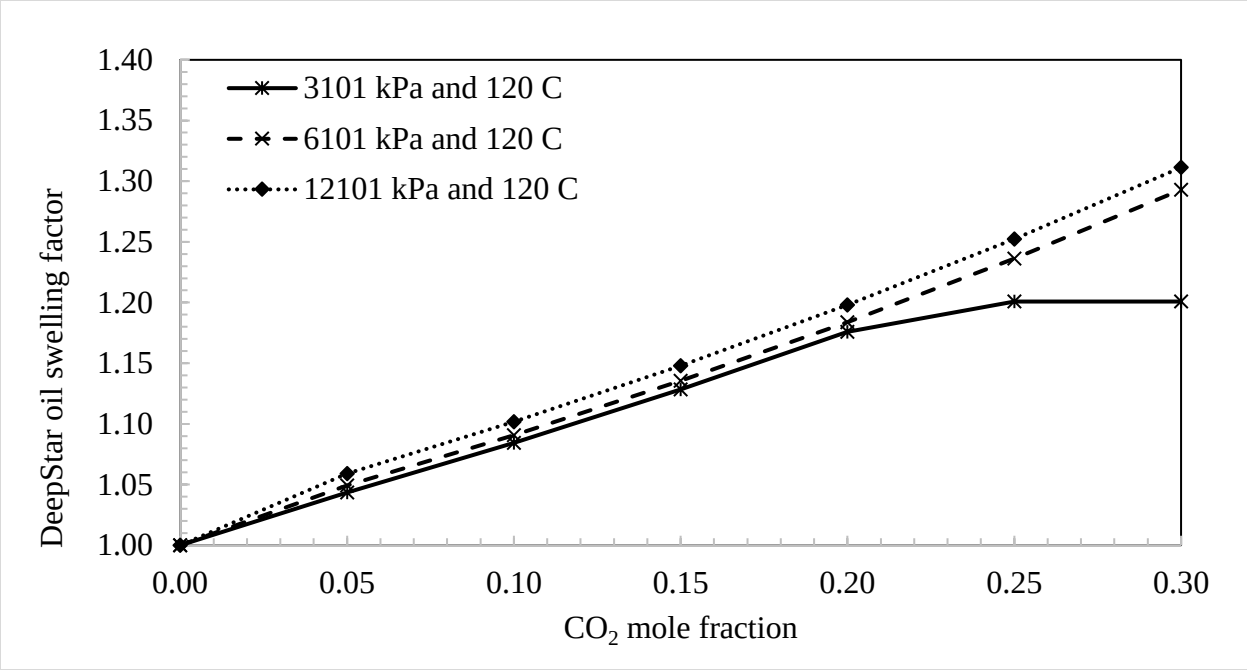

Figure 3-15 DeepStar oil swelling factor under different CO_2 concentrations and pressures.

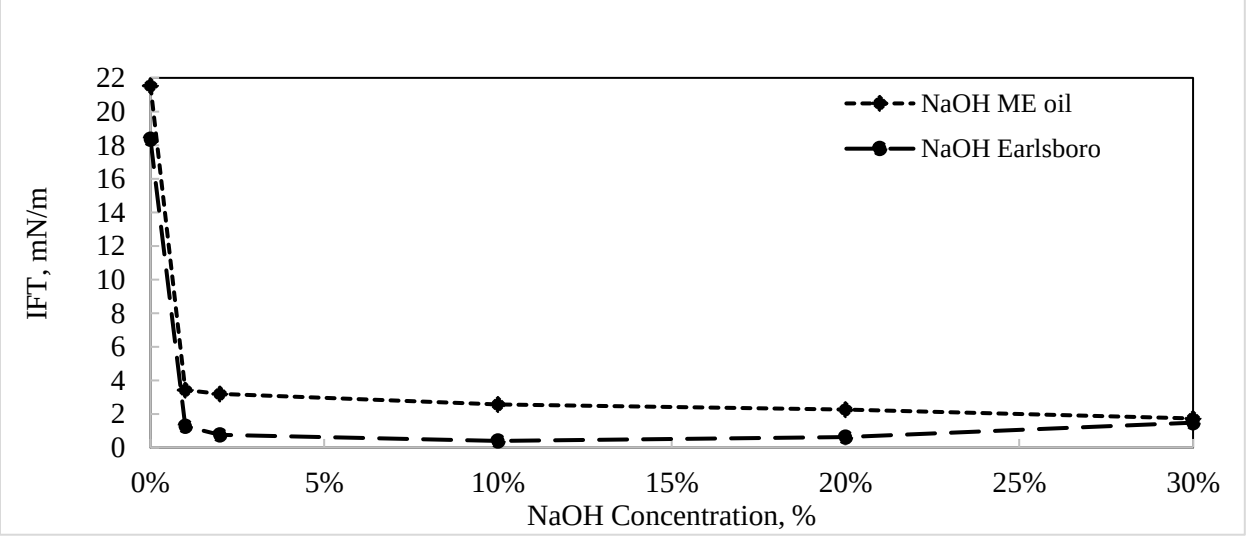

Figure 3-16 Measured Interfacial tension of Earlsboro oil sample under different sodium hydroxide concentration [14]

One of the objectives of history matches the laboratory experiments was to validate the synergetic mechanism and to quantify contributions of two ICE synergetic mechanisms in terms of recovery factors. The contribution of oil swelling and viscosity reduction to the recovery was

quantified with reaction kinetics only, whereas ammonia alkali (in-situ surfactant) was quantified by modifying relative permeability endpoints and oil/water relative exponents.

3.4. 3D Sector Model

The 1D mechanistic numerical models were upscaled to a 3D quarter 5-spot model (1 injector and 1 producer wells and they are positioned diagonally in a square). The model parameters are provided in Table 3-14:

Table 3-14 3D quarter 5-spot grid and rock properties

Grid and Rock Properties	
Property	Value
Grid Dimensions (x*y*z)	44*44*4
X/Y-direction block size (ft)	15
Porosity (frac)	0.15
Permeability (x, y and z)	200 mD
Water saturation	0.40
*Thickness (ft)	15.00
Depth (ft)	4000.00
Area (acres)	10.00
Original Oil In-place (OOIP), MMBBL	0.42
Reservoir Temperature (°F)	248
Reservoir Pressure (psia)	1500

**Thickness of each layer was 15ft.*

Building this model aims to simulate the urea flooding on a field scale and evaluate the prize of In-Situ CO_2 EOR. Initially, a base case without urea flooding was constructed, and after evaluating oil recovery, urea reaction was incorporated for In-Situ CO_2 EOR (ICE). The 3D view of the quarter 5-spot field model is shown in Figure 3-17:

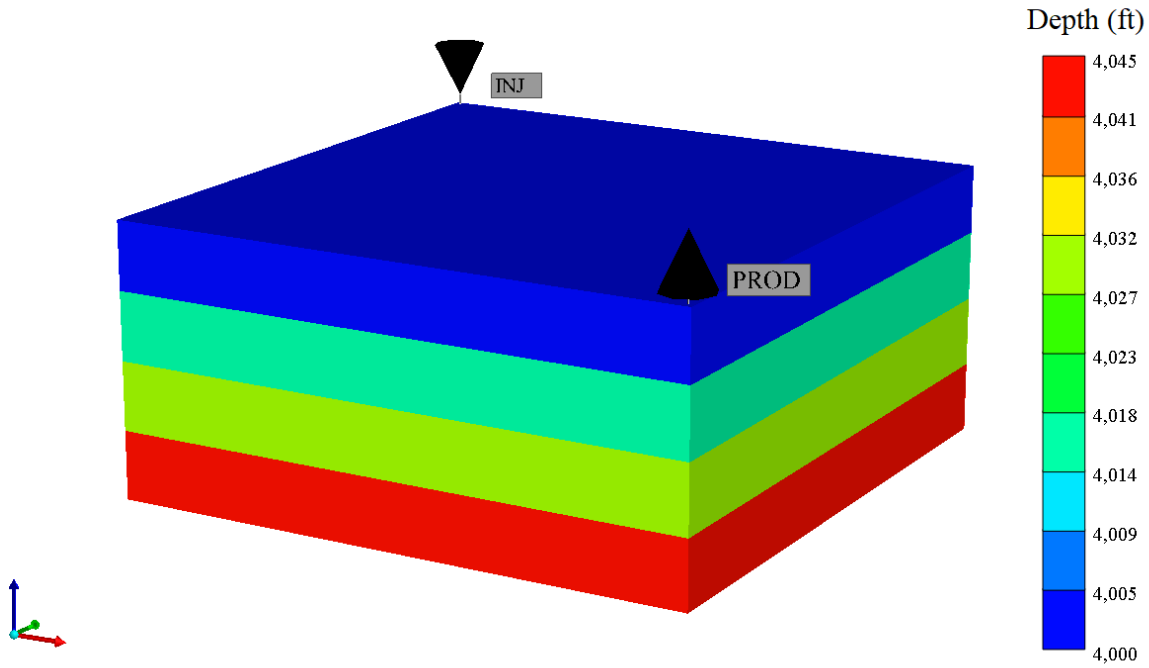

Figure 3-17 3D quarter 5-spot field model

In the model, the oleic phase was characterized by EOS with three components: light hydrocarbon, medium hydrocarbon, and heavy hydrocarbon, and EOS is from CMG-STARS SPE-003 (SPE comparative solution for steam drive simulation) template. The properties of oleic components are provided in Table 3-15:

Table 3-15 The properties of oleic components in the 3D quarter 5-spot sector model

Properties of Oleic Components in 3D Sector Model				
Component	Critical Pressure (psi)	Critical Temperature (F)	Mol.Wt (lb/lbmole)	Density (lb/ft^3)
Light Oil	225	800	250	52.30
Medium Oil	140	950	450	57.65
Heavy Oil	100	1000	600	61.20

The viscosity of oleic components was taken from a similar template; however, mixture viscosities were estimated using equations 3-6. The viscosity of light, medium, and heavy oil at different temperatures is provided in Table 3-16:

Table 3-16 The viscosity of light, medium, and heavy oleic phase components at different temperatures

Viscosities of Light, Medium, and Heavy oleic components CMG-STARS SPE Template						
	Viscosity (cp)					
Oleic Component	24°C	38°C	93°C	149°C	177°C	260°C
Light Oil	2.33	1.99	1.14	0.71	0.57	0.32
Medium Oil	10.58	9.06	5.18	3.21	2.58	1.45
Heavy Oil	5780.00	1380.00	47.00	8.50	5.20	2.50

Additionally, similar reaction kinetics were used, based on optimization to produce the number of CO_2 moles. The molar calculations were also performed to quality check the base case with urea hydrolysis reaction. The base case was run for sixty (60) days without any shut-in and controlled the model with injection pressure. The molar calculations of base case with urea flooding at 500 bbls/d injection rate are provided in Table 3-17.

Table 3-17 The urea molar calculations for the 3D sector model

Molar Calculations for 3D Field Case				
Urea mole fraction	Urea (ft3/day)	Urea (lb/day)	Urea (moles/day)	Urea Total (moles)
6%	168	13986	233	14219
14%	393	32635	544	33179
21%	590	48952	816	49768
28%	786	65269	1088	66357
35%	983	81587	1360	82946

After building the 3D a quarter 5-spot field model and incorporating the required data of urea hydrolysis reaction, the base case with urea flooding was evaluated based on oil recovery and the base case with water/brine flooding. After comparing base cases, a sensitivity analysis was

performed based on 1) Injection rate; 2) Reservoir Temperature; 3) Shut-in/No-Shu-in; and 4) urea concentration. An optimized scenario was selected based on the sensitivity analysis, and the prize of In-Situ CO_2 EOR (ICE) was determined. The results and observation of the 3D quarter 5-spot field model are discussed in Chapter 4 Results and Observations.

Chapter 4: Simulation Results and Discussions

The numerical modeling schemes involved in this study were explained in Chapter 3 Numerical Modeling of Urea Injection. In this chapter, the results and observations of each numerical mechanistic model will be discussed.

4.1. 1D Numerical Mechanistic Model

The 1D numerical mechanistic model was built to model the synergetic mechanisms of ICE. The urea hydrolysis reaction kinetics were studied thoroughly before building the model. Based on urea hydrolysis reaction kinetics provided by researchers [5,17,18,19], the model was constructed, and reaction data was incorporated. However, reaction kinetics provided by researchers [5,17,18,19] did not generate a sufficient amount of CO_2 moles in the numerical simulation model based on molar calculations.

To produce the desired CO_2 moles, the reaction kinetics, i.e., the activation energy (kJ/mol) and pre-exponential factor, A, (also known as reaction frequency factor, 1/min) was modified in the model. Based on 35 wt.% urea concentration, the numerical model should produce 0.24 moles of CO_2 and determined activation energy of 84.50 kJ/mole and pre-exponential factor of 7E+09 1/min were used to produce the desired CO_2 moles. The urea solution was continuously injected in the model; hence, the CO_2 moles increased with time. Figure 4-1 shows the CO_2 mole fraction in oil at different pore volumes injected in the reservoir.

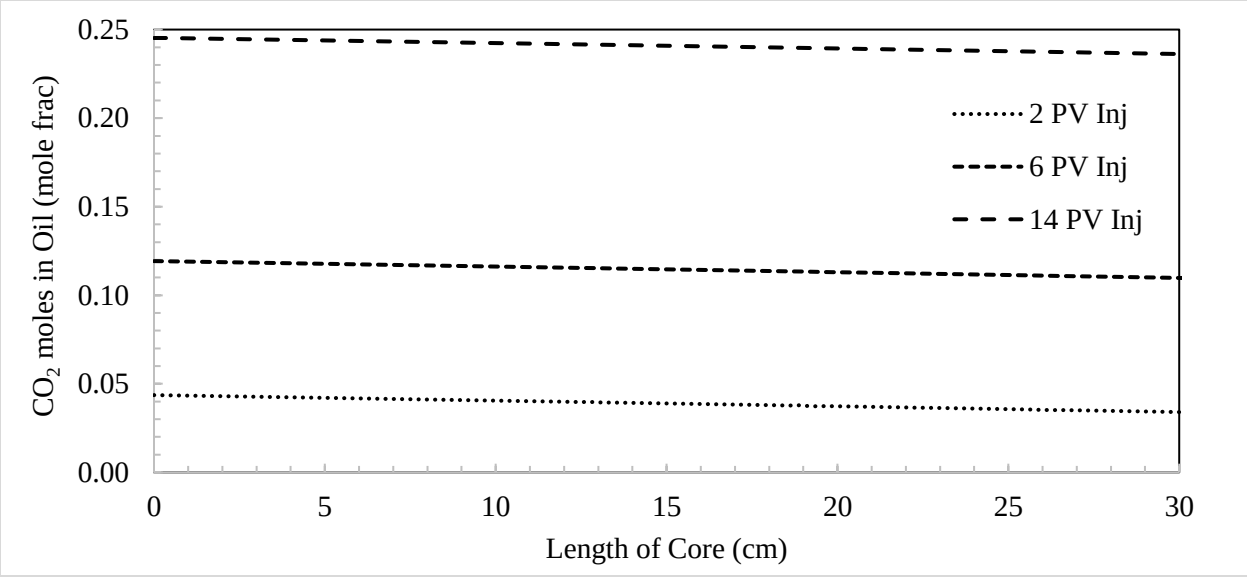

Figure 4-1 The produced number of CO_2 moles dissolved in the oil at different pore volume injection.

After successfully developing the workflow to model the synergetic mechanisms of ICE, the following were the results and observations based on the 1D mechanistic numerical model:

1. Oil swelling has a nearly linear relationship with the amount of CO_2 dissolved in the oil phase. Up to 25% oil swelling was observed when 0.24 moles of CO_2 dissolved in oil. The oil swelling factor of octane based on EOS was showed in Figures 2-10 and 3-6.
2. Due to oil swelling, a 0.16% increase in oil saturation was also observed after injecting 14 pore volumes of water and urea solution.
3. Octane viscosity was reduced from 0.21 cp to 0.12 cp due to mixing with CO_2, a viscosity reduction of 43% in oil viscosity. Figure 4-2 shows the octane viscosity at different PV injected of urea.
4. The incremental oil recovery due to oil swelling and viscosity reduction was 8.50% after urea injection in the mechanistic numerical model.

5. The octane was used as the oleic phase in the 1D mechanistic numerical model, and it was assumed that there was no petroleum acid in the octane. However, IFT reduction was observed due to reduced oil viscosity, and incremental recovery due to reduction in IFT was 6.61% in the numerical mechanistic model. Therefore, due to synergetic mechanisms of oil swelling, viscosity, and IFT reduction, a total incremental recovery of 15.11% was observed.

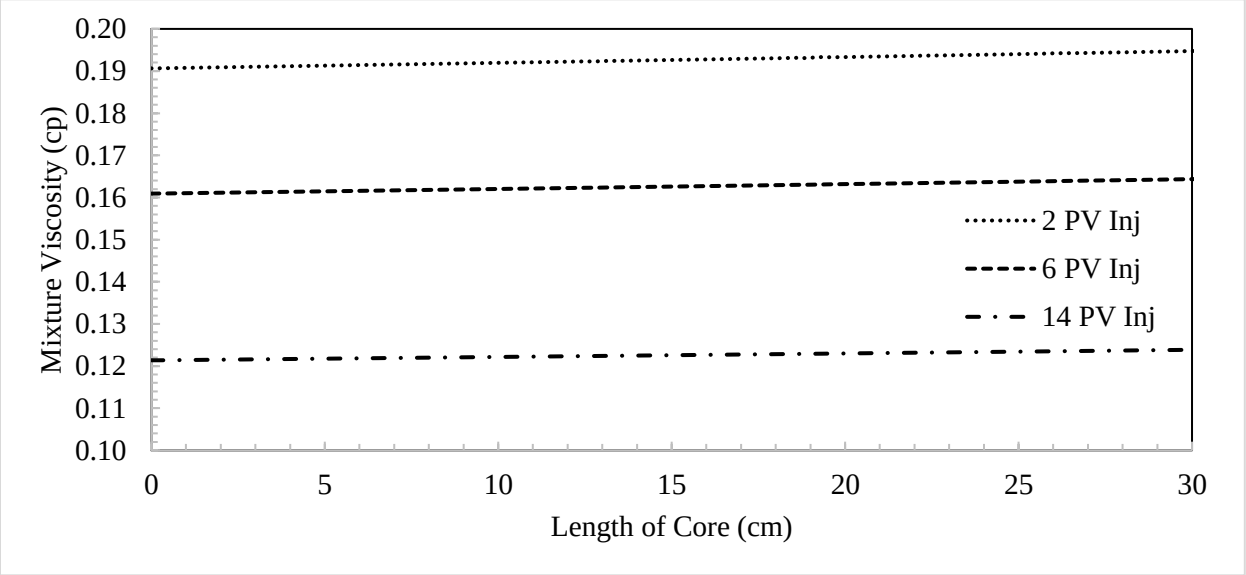

Figure 4-2 The CO_2 and octane mixture viscosity in the core at different PV injected of urea.

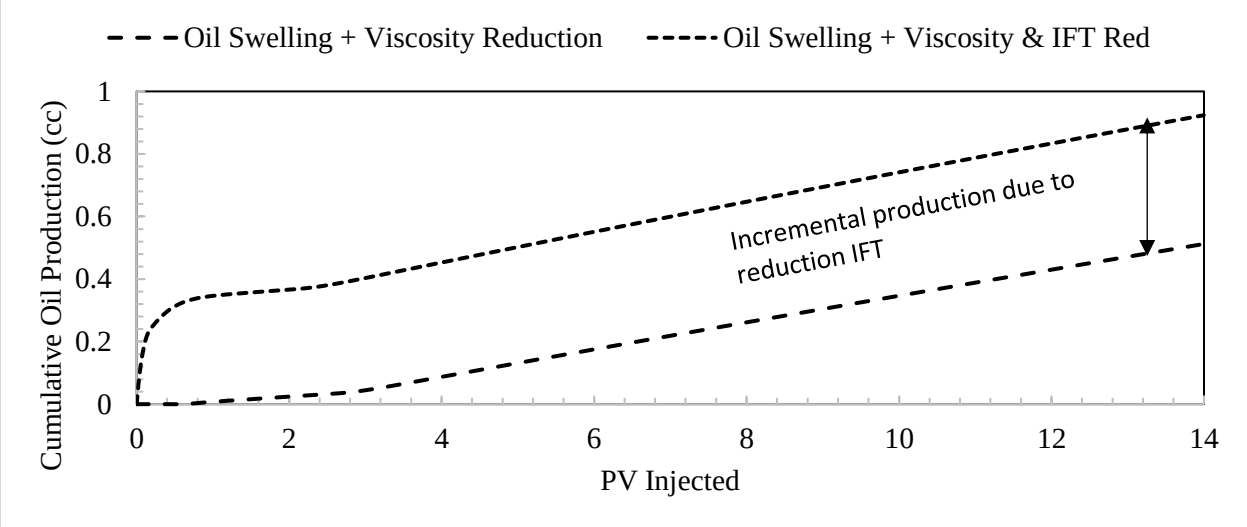

Figure 4-3 The cumulative oil produced due to oil swelling, and viscosity and IFT reduction synergetic mechanisms.

Figure 4-3 shows the cumulative production due to oil swelling and viscosity reduction, the combined effect of oil swelling, viscosity, and IFT reduction at different pore volumes of urea injection.

4.2. 1D Laboratory Numerical Models

1D laboratory experiments on ICE were performed by Wang [5] and were used to validate the synergetic mechanisms modeled in the 1D mechanistic numerical model in this study. Laboratory experiments with different oil compositions and residual oil saturations were chosen for history matching. The measured oil saturations versus pore volumes of injection were history-matched for three different tests: Test-1 was performed with Dodecane, Test-2 was performed with Earlsboro oil, and Test-3 was performed with DeepStar oil. The model and fluid properties for three different oils are provided in Chapter 3. The results and observations of each test are provided below:

4.2.1. Test-1 – Dodecane

1. The urea reaction kinetics previously matched in the 1D mechanistic numerical model was used in this case, but it did not produce the desired amount of CO_2 with the 35 wt.% urea concentration that was used in the laboratory experiments. Based on molar calculations, the urea reaction produced 0.53 moles of CO_2. The increase CO_2 moles were due to different injection cycles of urea and brine and shut-in in between injection cycles. In the simulation, the activation energy was set 92 kJ/mole and a pre-exponential factor to 8E+09 min^{-1} was used to generate the desired CO_2 moles for the history matching. Figure 4-4 shows the concentration of CO_2 in the dodecane at different PV injections. To history match the Test-1, reaction kinetics were modified. Figure 4-4 shows that CO_2

mole fraction in dodecane increases significantly from 6 PV to 11 PV injection which is due to shut-in but urea reaction in the core continued to produce CO_2.

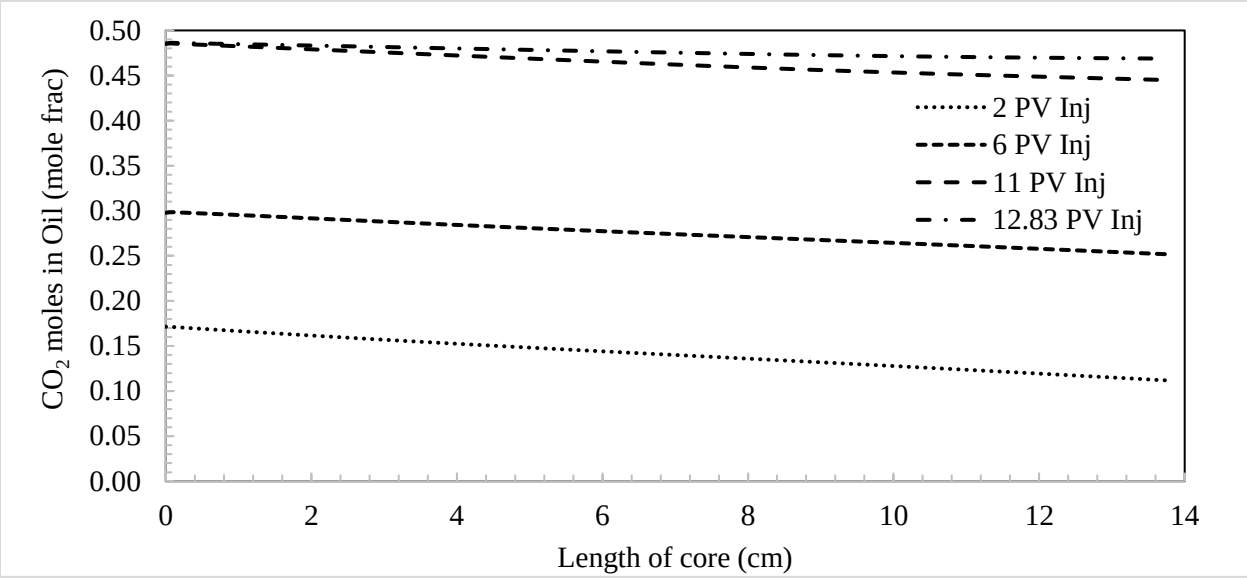

Figure 4-4 The produced CO_2 moles dissolved in the oil at different pore volume injection.

2. It was assumed that there was no petroleum acid in dodecane. Therefore, only oil swelling and viscosity reduction synergetic mechanisms present in Test-1. Based on the CO_2 concentration in dodecane, the oil swelling was ~50%, and incremental oil recovery due to oil swelling and viscosity reduction was quantified as 17.96% in the Test-1. The dodecane viscosity was reduced from 0.41 cp to 0.10 cp, representing 76% reduction in oil viscosity. Figure 4-5 shows the dodecane viscosity at different PV injected of urea. Similarly, figure 4-5 shows the mixture viscosity reduces significantly from 6 PV to 11 PV injection which is due to chemical reaction continuation during shut-in.
3. No direct measurement of relative permeability was available in the laboratory experiments of ICE. Relative permeability data was not modified for history matching in

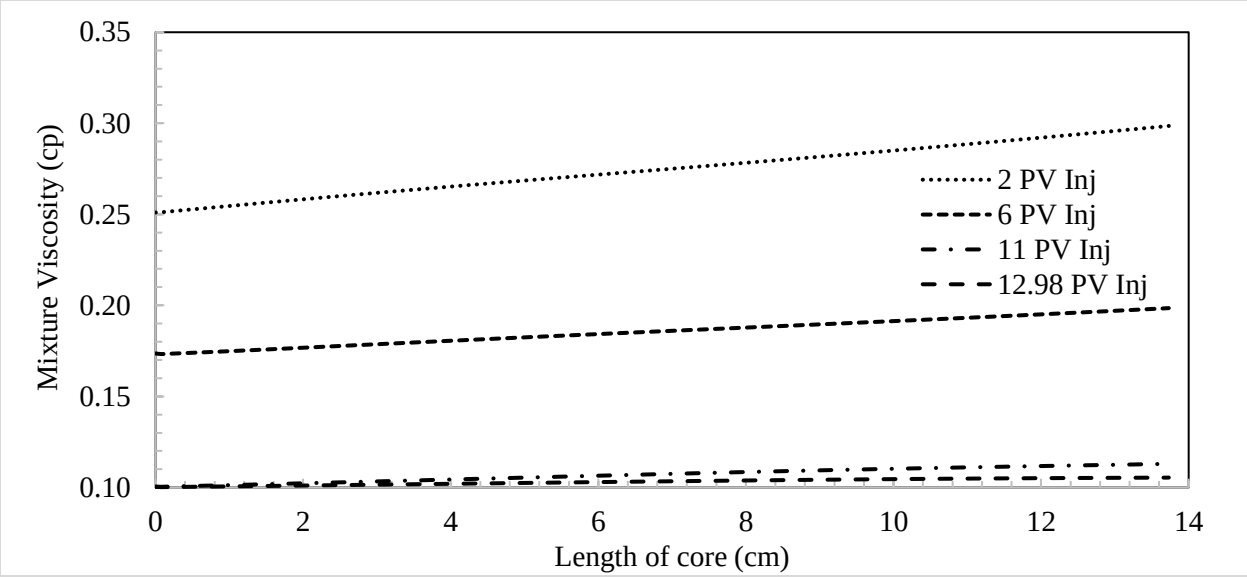

Figure 4-5 The CO_2 and dodecane mixture viscosity in the core at different PV injected of urea.

the Test-1, and the urea reaction kinetics proved to be the main uncertainty in this case. The main synergetic mechanisms in this case were oil swelling and viscosity reduction.

4. However, Li [14] measured the IFT of dodecane under different urea concentrations as shown in Figure 3-6 in Chapter 3 with possible reasons. After incorporating the dodecane IFT measured by Li [14] in the model, the incremental recovery due to IFT reduction was observed as 0.20% after modifying relative permeability, and the comparison of relative permeability is shown in Figure 4-7. Test-1 history match is shown in Figure 4-6.
5. The ICE synergetic mechanisms of oil swelling and viscosity reduction were validated in this case, but the reduction of IFT and modifying the relative permeability may not be accurate and requires further laboratory measurements. Additionally, it can be observed in Figure 4-6 that initial measured data is not very well matched with simulated data

which may be due to uncertainty in the relative permeability of the sample, and this rock sample is believed to be highly water-wet.

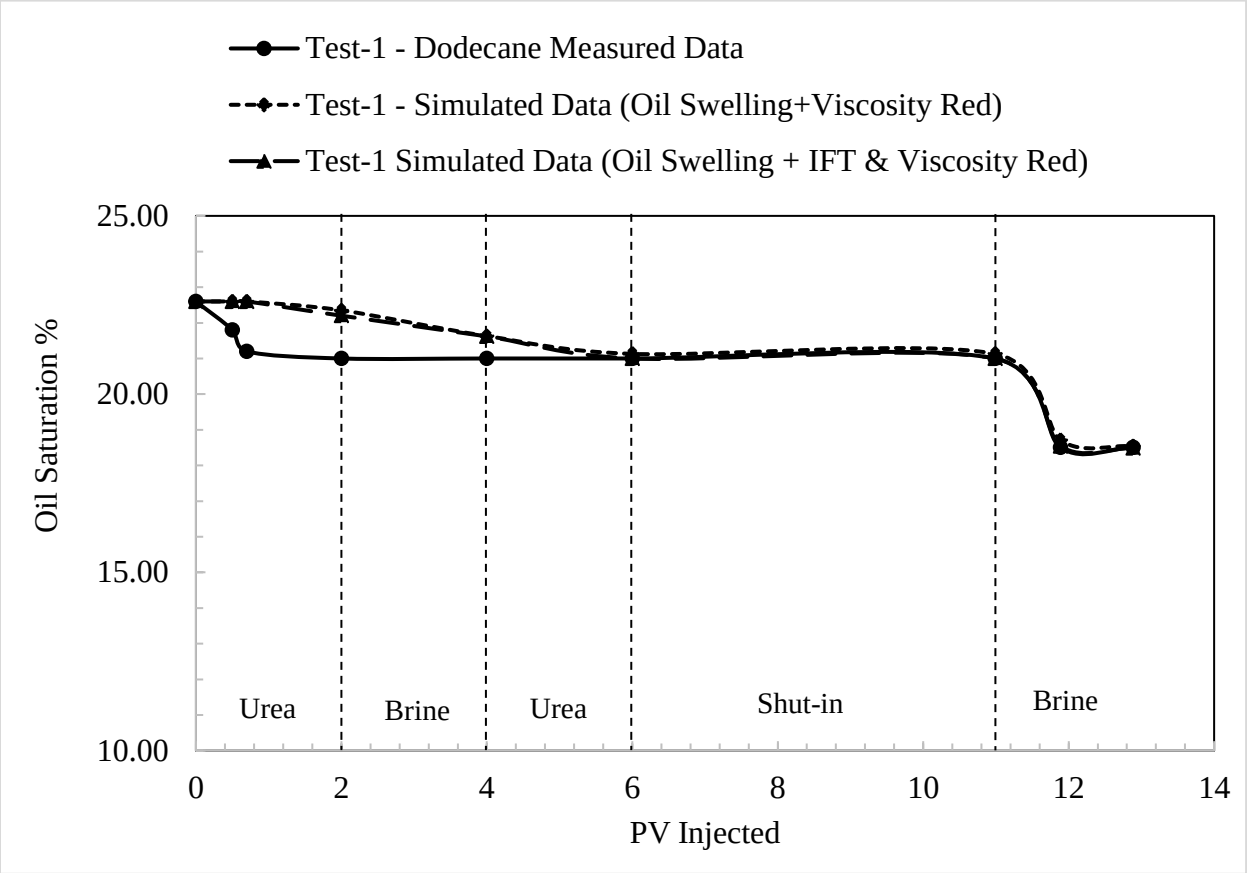

Figure 4-6 Test-1 dodecane history match and validation of synergetic mechanisms of ICE

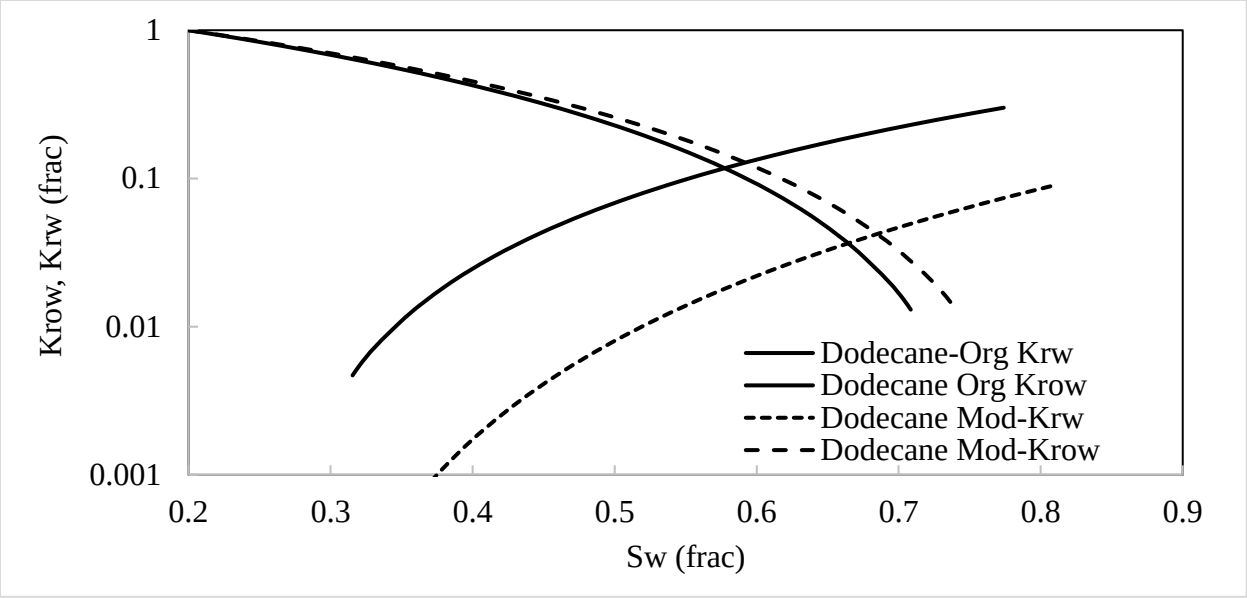

Figure 4-7 Original and modified relative permeability data used in Test-1.

4.2.2. Test-2 – Earlsboro oil

In this case, the urea reaction kinetics used the same value as in Test-1 since the temperature was the same. The activation energy of 92 kJ/mole and pre-exponential factor of 8E+09 min^{-1} was used in the history matching of all three tests. The results and observations of Test-2 are provided below:

1. The urea reaction kinetics in the model could generate 0.15 moles of CO_2 which accounts for 3.78% incremental recovery due to oil swelling and viscosity reduction. Figure 4-8 shows the concentration of CO_2 in Earlsboro oil at different PV injection of urea without modifying relative permeability.
2. After modifying reaction kinetics, the swelling factor and mixture viscosity was affected, and the model did not produce sufficient CO_2 moles compared to molar calculations based on urea concentration and injection rate. However, after modifying the relative permeability endpoints to incorporate the contribution of IFT reduction and wettability alteration in the model, the produced CO_2 moles increased to 0.40 which account for

44.39% incremental recovery due to the combined effect of oil swelling, viscosity and IFT reduction, and wettability alteration. The increase in CO_2 number of moles produced may be due to more mobile oil allowed to flow after modifying relative permeability endpoints. Li [14] measured the IFT of Earlsboro oil under different sodium hydroxide concentrations and reported the petroleum acid content in Earlsboro oil as high. Therefore, it was believed that incremental recovery due to the synergetic mechanism of wettability alteration because of ammonia alkali is significant and contributes to more In-Situ CO_2 production. Figure 4-8 shows the concentration of CO_2 in Earlsboro oil after modifying relative permeability endpoints at different PV injections of urea.

3. It was believed that reduction of IFT and relative permeability endpoints allow more oil to mobilize in the porous media, produces more CO_2 which partitions into oil and contributes to incremental oil recovery. Therefore, the recovery due to oil swelling and viscosity reduction can be higher than 3.78%. The relative permeability endpoints were reduced by 38% as compared to the original endpoint saturation. Since, there was no direct measurement of relative permeability available, the relative permeability of oil and water, and endpoint saturations were modified based on trial and error to history match the Test-2.
4. The viscosity reduction of Earlsboro oil after modifying relative permeability endpoints and at 0.40 moles of CO_2 dissolved in Earlsboro oil was 79%, Earlsboro oil viscosity reduced from 1.03 cp to 0.21 cp. The mixture viscosity of Earlsboro oil and CO_2 is shown in Figure 4-10. Additionally, the residual oil saturation after urea flooding reduced from 50% to 30%.

5. Test-2 was history matched with measured oil saturation versus pore volumes injected with less than 5% error. The history matching of Test-2 is shown in Figure 4-11. It can be observed in the Figure that with modifying relative permeability of oil and water, and endpoints, the simulated data is too far from measured data. The initial part of history matching (up to 2 PV injected) shows a higher decrease in oil saturation as compared to measured oil saturation which may be due to higher uncertainty in water permeability.
6. It was also observed that relative permeability was highly CO_2 concentration-dependent in all lab cases due to cyclic injection of brine and urea based on mismatches in the history matching. Relative permeability showed dynamic behavior while history matching the observed data due to switching of injection fluid from urea to brine. Urea injected affected the flow of water and oil in porous media which may be the reason for the concentration dependency of relative permeability. However, the simulator does not account for the concentration effect of relative permeability for different phases of injection, it only has one relative permeability dataset for all fluids in the reservoir. The original and modified relative permeability data used in Test-2 is shown in Figure 4-12.

7. The contributions of synergetic mechanisms of ICE in terms of recovery factor in the Test-2 were, recovery due to oil swelling and viscosity reduction was higher than 6.39% and recovery due to IFT reduction and wettability alteration was 38%.

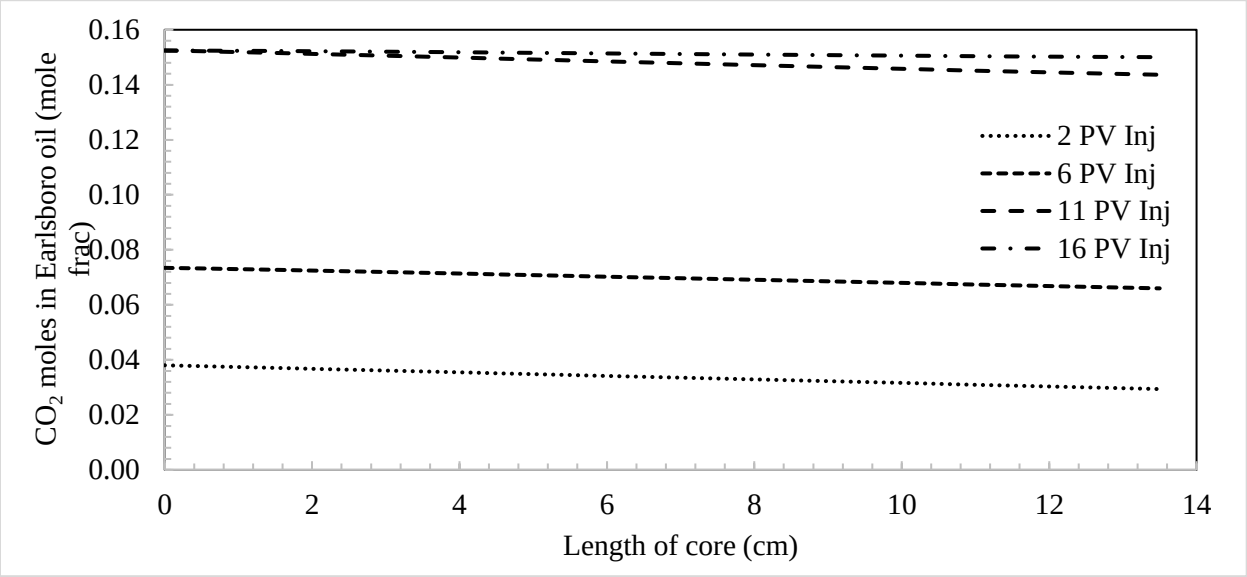

Figure 4-8 The produced CO_2 moles dissolved in the Earlsboro oil at different pore volume injection without modifying relative permeability.

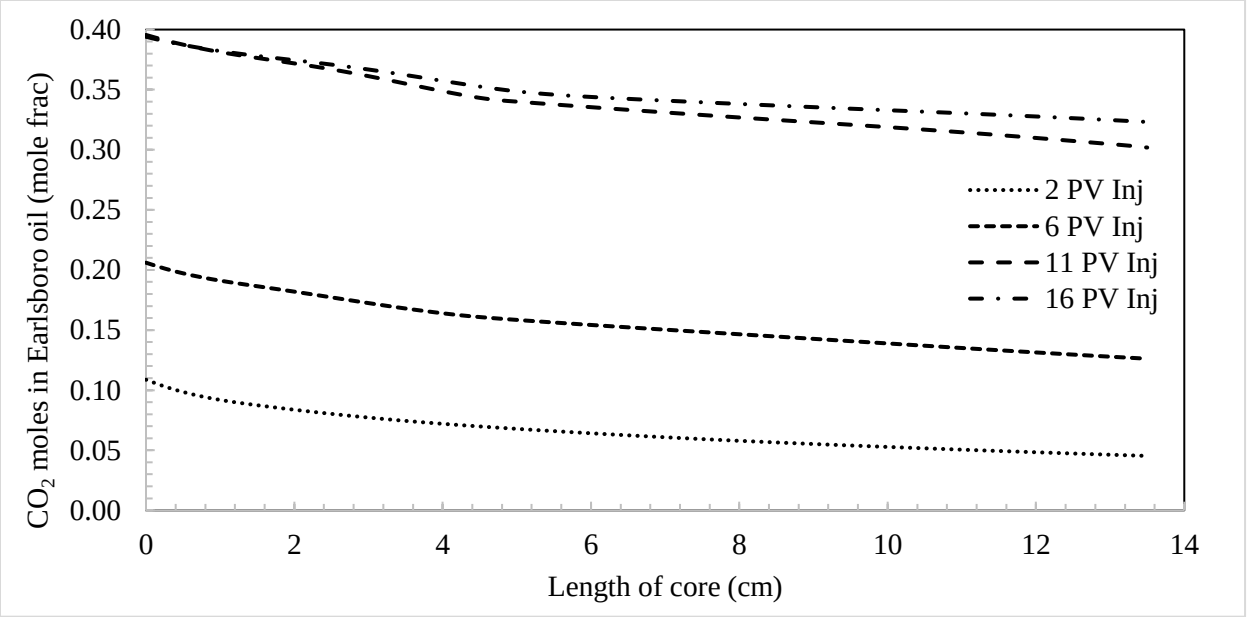

Figure 4-9 The produced CO_2 moles dissolved in the Earlsboro oil at different pore volume injection after modifying relative permeability.

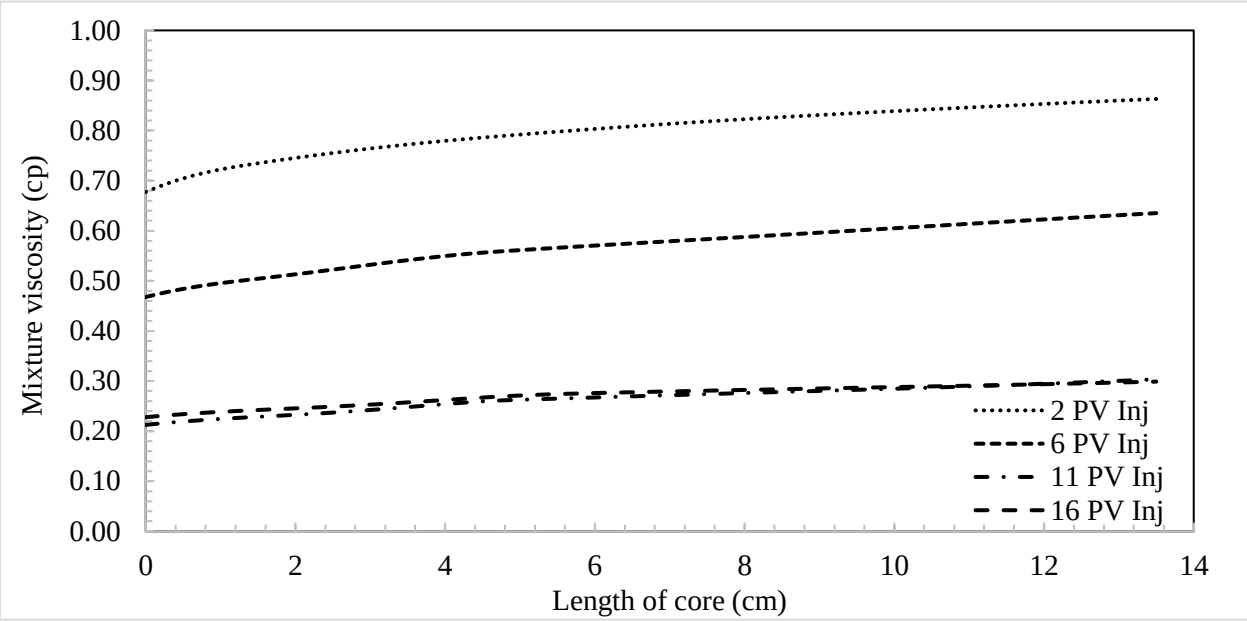

Figure 4-10 The CO_2 and Earlsboro oil mixture viscosity in the core at different PV injected of urea.

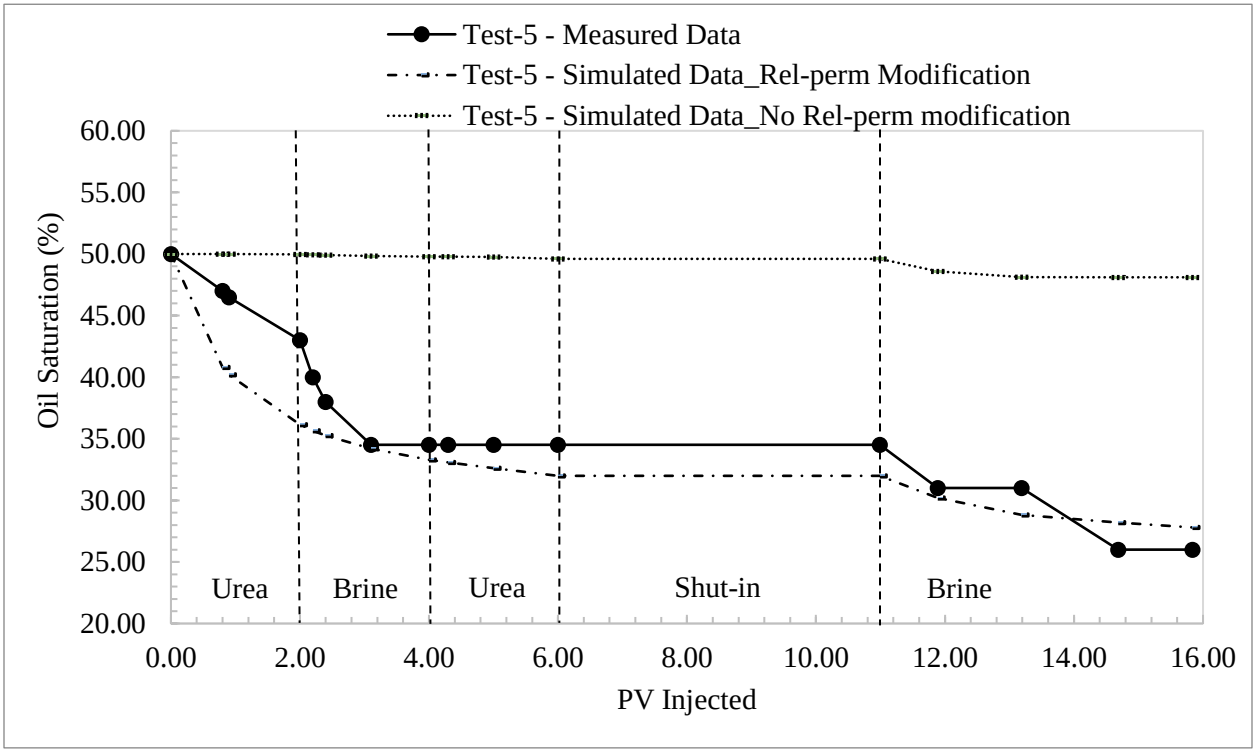

Figure 4-11 Test-2 Earlsboro oil history match and validation of synergetic mechanisms of ICE

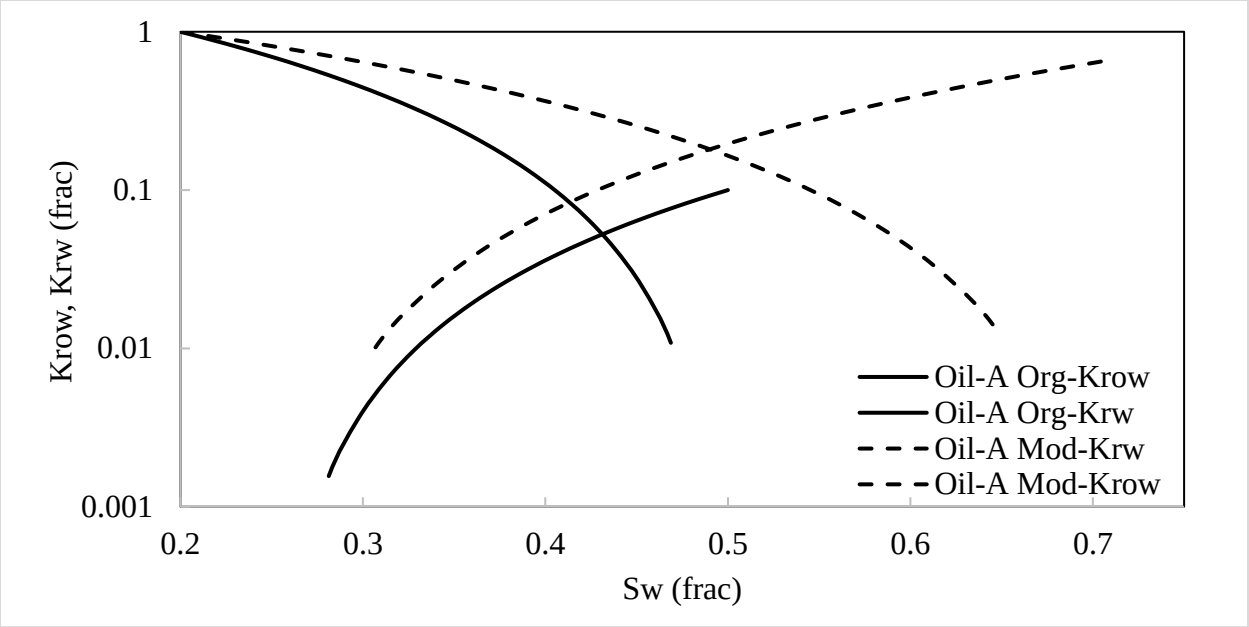

Figure 4-12 Original and modified relative permeability data used in Test-2.

4.2.3. Test-3 – DeepStar oil

DeepStar oil used in Test-3 was the heaviest (in terms of viscosity) and the history matching behavior of this test was different from the previous two tests. The urea reaction kinetics were set to have an activation energy of 92 kJ/mole and a pre-exponential factor of 8E+09 min^{-1} determined from the previous simulation. History matching results and observations are provided below:

1. In this test, the urea reaction produced 0.41 moles of CO_2, whereas based on molar calculations, it should produce 0.53 moles of CO_2. The reason to analyze the produced CO_2 moles based on urea reaction kinetics without modifying the relative permeability was to evaluate how much urea reaction kinetics alone contribute to oil swelling and viscosity reduction. This resulted in different behavior of urea hydrolysis and CO_2 partitioning in different reservoir fluid compositions. Figure 4-13 shows the

concentration of CO_2 in DeepStar oil at different PV injection of urea without modifying relative permeability.

2. To obtain a good history match of measured versus simulated data, the relative permeability of oil and water and endpoints were modified. Modifying relative permeability served the purpose of IFT reduction due to viscosity reduction and wettability alteration. After modifying relative permeability, the produced CO_2 moles also increased to 0.50 from 0.40 which depicted that increasing the oil relative permeability causes the urea reaction to produce more CO_2, swell the oil, and reduce the oil viscosity. Figure 4-14 shows the concentration of CO_2 in DeepStar oil at different PV injections of urea after modifying relative permeability. The original and modified relative permeability data used in Test-3 is shown in Figure 4-16.
3. The incremental oil recovery due to oil swelling and viscosity reduction without modifying relative permeability was 11.36%. In contrast, modifying relative permeability to incorporate IFT reduction and ammonia alkali synergetic mechanism, the incremental recovery increased to 24.75%.
4. The viscosity of DeepStar oil reduced from 3.07 cp to 0.27 cp; a reduction of 91% was observed during the history matching of Test-2, and this contributed to significant incremental oil recovery. The mixture viscosity of DeepStar oil and CO_2 is shown in Figure 4-15. Additionally, the residual oil saturation reduced from 29% to 26% in this test.

5. Test-3 history match of oil saturation versus pore volumes injected is shown in Figure 4-17. It can be observed that in Figure that oil saturation is not very well matched from 2 to 10 PV injected. Due to the injection of different fluids in cycles and relative permeability, it seemed to be CO_2 concentration-dependent. The direct measurement of relative permeability of oil and water during injection of brine and urea was not available. Therefore, this best match was obtained based on a trial-and-error approach. Additionally, it was also observed that the cycle of brine injection assisted in recovering the mixture of oil and CO_2, having lower viscosity as compared to original reservoir oil. A similar approach was followed while designing the optimized urea flooding scenario on a field scale.

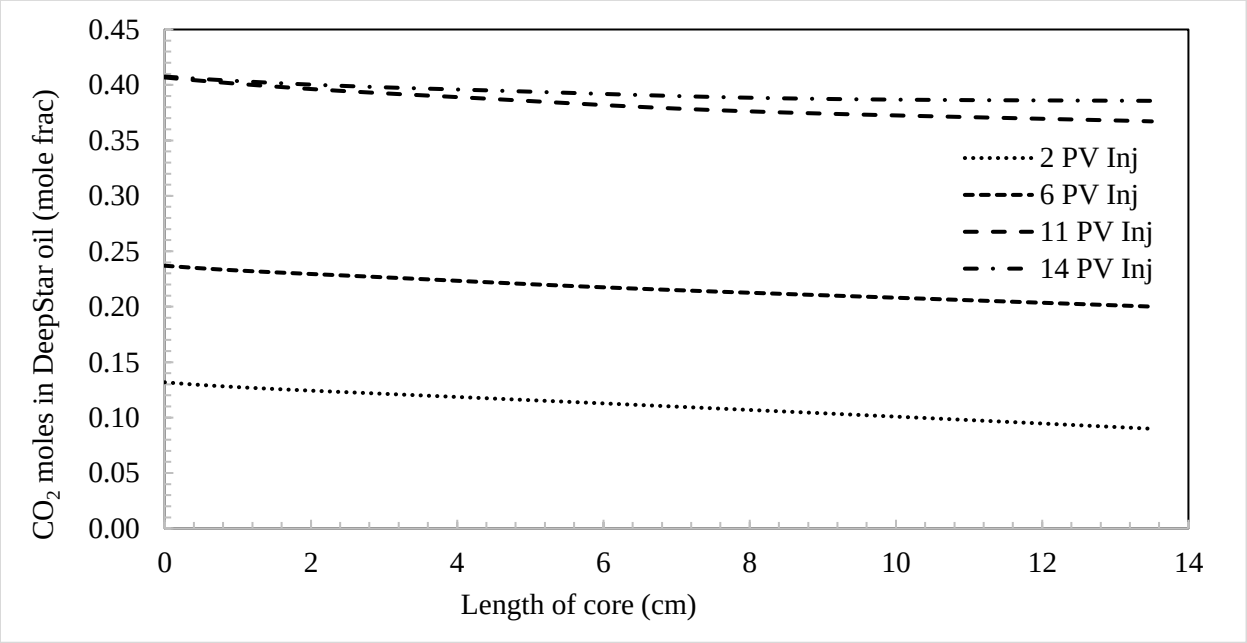

Figure 4-13 The produced CO_2 moles dissolved in the DeepStar oil at different pore volume injection without modifying relative permeability.

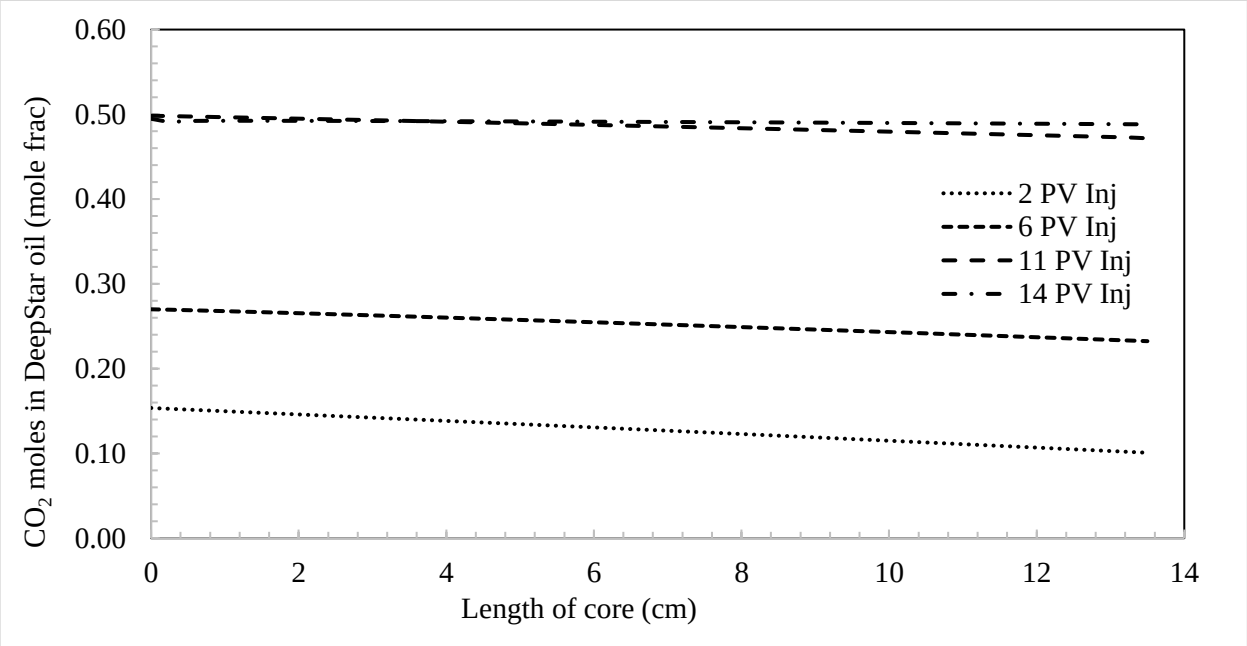

Figure 4-14 The produced CO_2 moles dissolved in the DeepStar oil at different pore volume injection after modifying relative permeability.

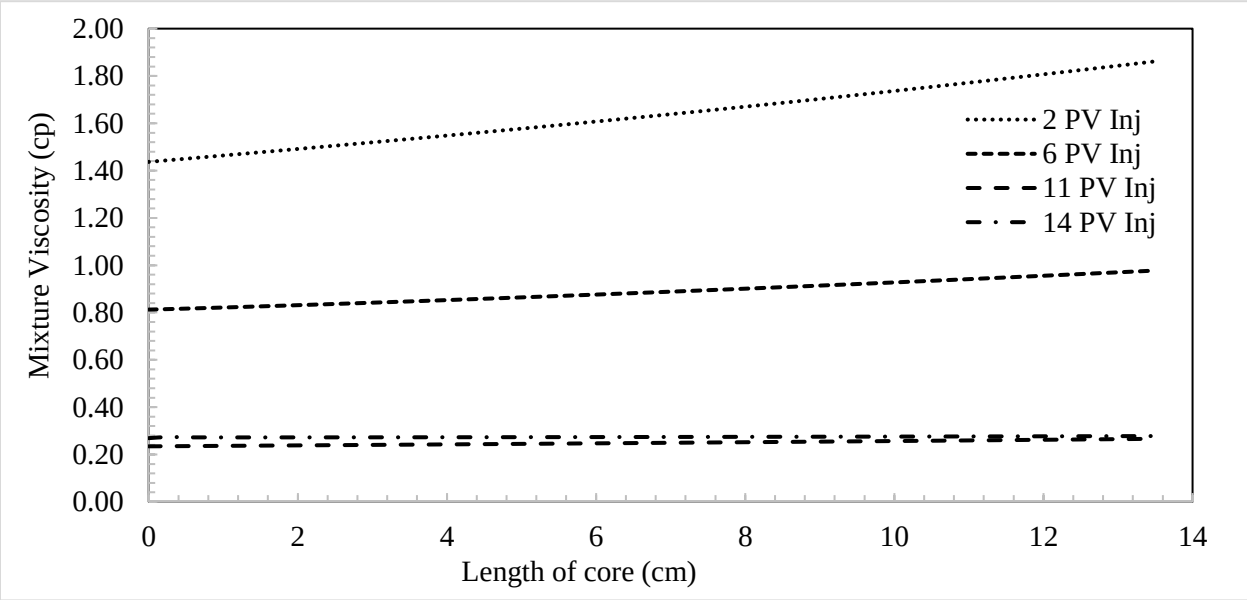

Figure 4-15 The CO_2 and DeepStar oil mixture viscosity in the core at different PV injected of urea.

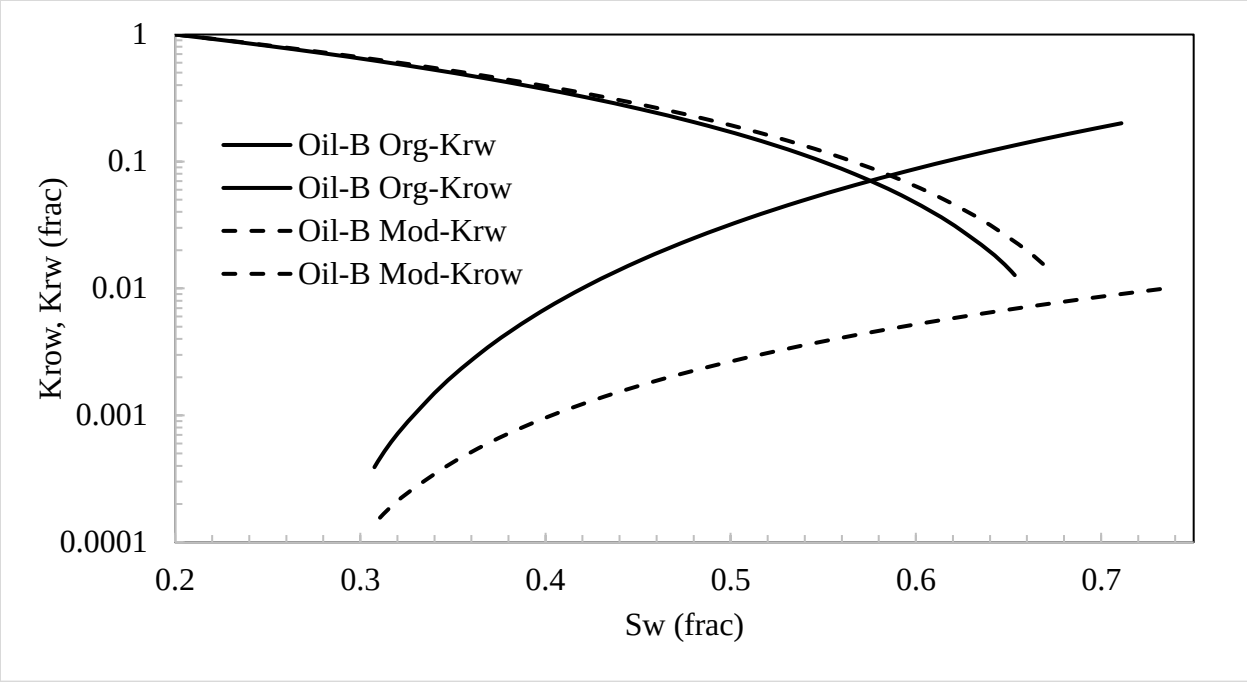

Figure 4-16 Original and modified relative permeability data used in Test-3.

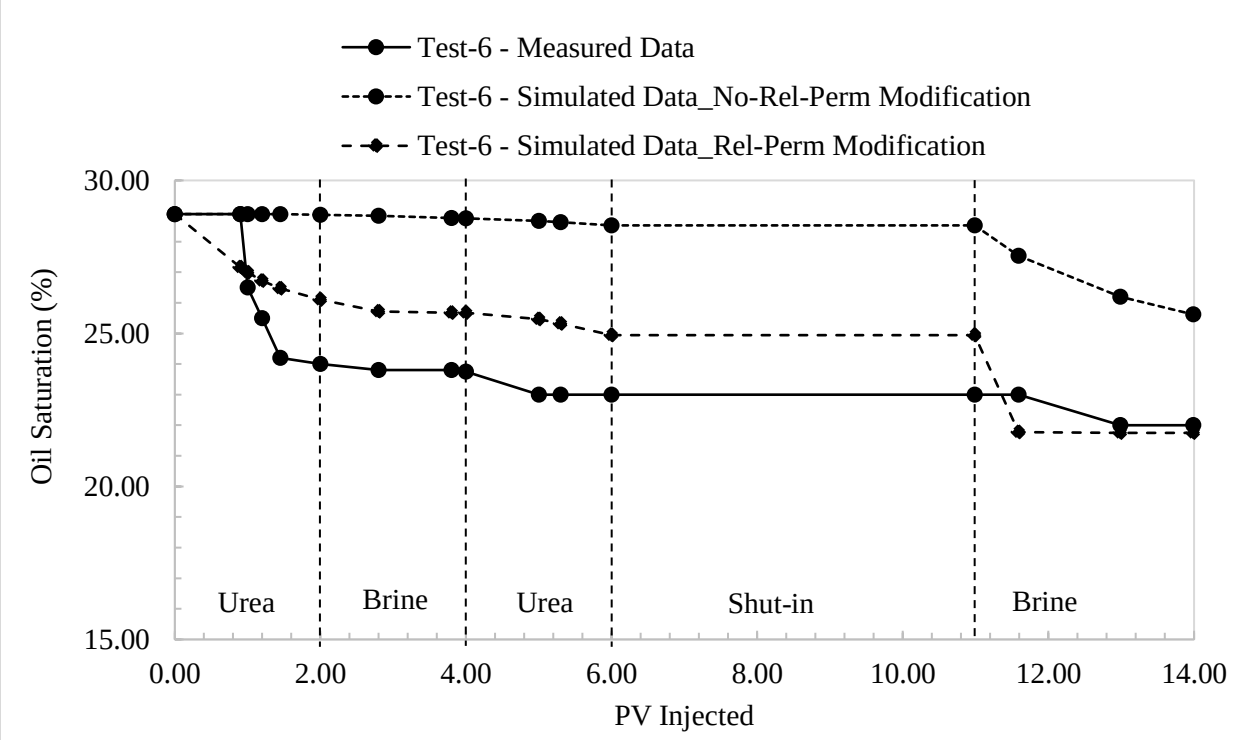

Figure 4-17 Test-3 DeepStar oil history match and validation of synergetic mechanisms of ICE

4.3. 3D Sector Model

The objective of building a 3D model was to optimize the urea injection based on urea injection slug, shut-in duration, and urea concentration. Different scenarios were to evaluate the optimal urea injection scenario as compared to waterflooding. The waterflooding scenario was considered as Base Case. The production and injection constraints of the base case and urea injection cases are provided in Table 4-1.

Table 4-1 Production and Injection constraints used in 3D sector model.

Production /Injection Constraints	
Constraint	Value
Injection Rate (bpd)	2000
Injection Pressure (psi)	4000
Production Liquid Rate (bpd)	2000
*PV Injected	0.172
Reservoir Temperature (°F)	248
Reservoir Pressure (psi)	1500

**Actual PV injected can be different based on injection profile.*

The results and observations of sensitivity analysis and optimal urea flooding scenario are provided below:

1. The waterflooding base case showed a recovery of 9.79% after injecting 0.10 PV of water for two months. A continuous urea injection showed a recovery of 12% after injecting the 0.11 PV of urea and water for two months. This recovery was contributed by oil swelling and viscosity reduction synergetic mechanisms only. After incorporating ammonia alkali and IFT reduction mechanism, the incremental recovery increased by 3.10% to 15.10% after injecting 0.13 PV of urea and water.
2. I conducted sensitivities of injection rate, reservoir temperature, urea concentration, and shut-in/No shut-in. The determined rate is 2000 bbl/d injection rate, 248°F reservoir

temperature, 25 wt.% urea concentration, and shut-in cycle included based on a limited number of trials on the above parameters. Additionally, it was also observed that the higher the reservoir temperature, the higher would be the urea reaction rate and incremental recovery, but non-thermal simulation cases showed convergence issues, and oil recovery could not establish. Also, the shut-in cycle showed improved recovery due to urea reaction continuation in the reservoir and lesser injection urea which can be economical. The cyclic scenarios were further optimized with objectives functions of lesser injection of urea and higher incremental oil recovery as compared to waterflooding base case. The results of waterflooding base case, continuous urea injection case and cyclic urea injection and optimum case are provided in Table 4-2.

3. It was also observed from the results that in all cyclic injection cases, similar PV of water and urea injected more to be successful in incremental recovery. However, the main objective was to optimize incremental recovery based on the lesser mass of urea injection. The optimum case shows the incremental oil recovery of 3.48% compared to waterflooding with urea injection for five days only. In terms of incremental recovery in optimum cases, the contributions of synergetic mechanisms were 1.35% by oil swelling and viscosity reduction, and 2.13% by IFT reduction and wettability alteration. Figure 4-15 shows the concentration of CO_2 in the reservoir during urea injection and shut-in duration.

Table 4-2 The results of waterflooding base case, continuous and cyclic urea injection, and optimum case of 3D sector model

Results of Waterflooding, Continuous & Cyclic Urea Injection												
Case	Injection Strategy	Urea flooding slug size (days)	Shut-in (days)	Brine Flooding (days)	Urea concentration (wt.%)	Cumulative production (Bbl)	Oil Swelling and Viscosity Reduction Recovery Factor (%)	Total Recovery Factor (%)	Incremental recovery after waterflooding (%)	PV water injected	Cumulative Water Injected (Bbl)	Cumulative Water Produced (Bbl)
Waterflooding	Continuous	-	-	60	-	41023	-	9.79	-	0.10	68738	22996
Urea flooding	Continuous	60	-	60	35	64161	12.15	15.32	5.52	0.13	89013	25813
Case-1	Cyclic	15	5	10	35	46900	9.33	11.20	1.40	0.10	66700	17374
		10	10	10								
Case-2	Cyclic	10	10	40	35	51270	10.28	12.24	2.45	0.10	71511	19229
Case-3	Cyclic	30	10	20	35	52796	10.28	12.60	2.81	0.10	67369	19804
Case-4	Cyclic	20	20	20	35	41806	8.19	9.98	0.19	0.08	54208	15587
Optimum Case	**Cyclic**	**5**	**5**	**50**	**25**	**55613**	**11.14**	**13.28**	**3.48**	**0.12**	**81141**	**21083**

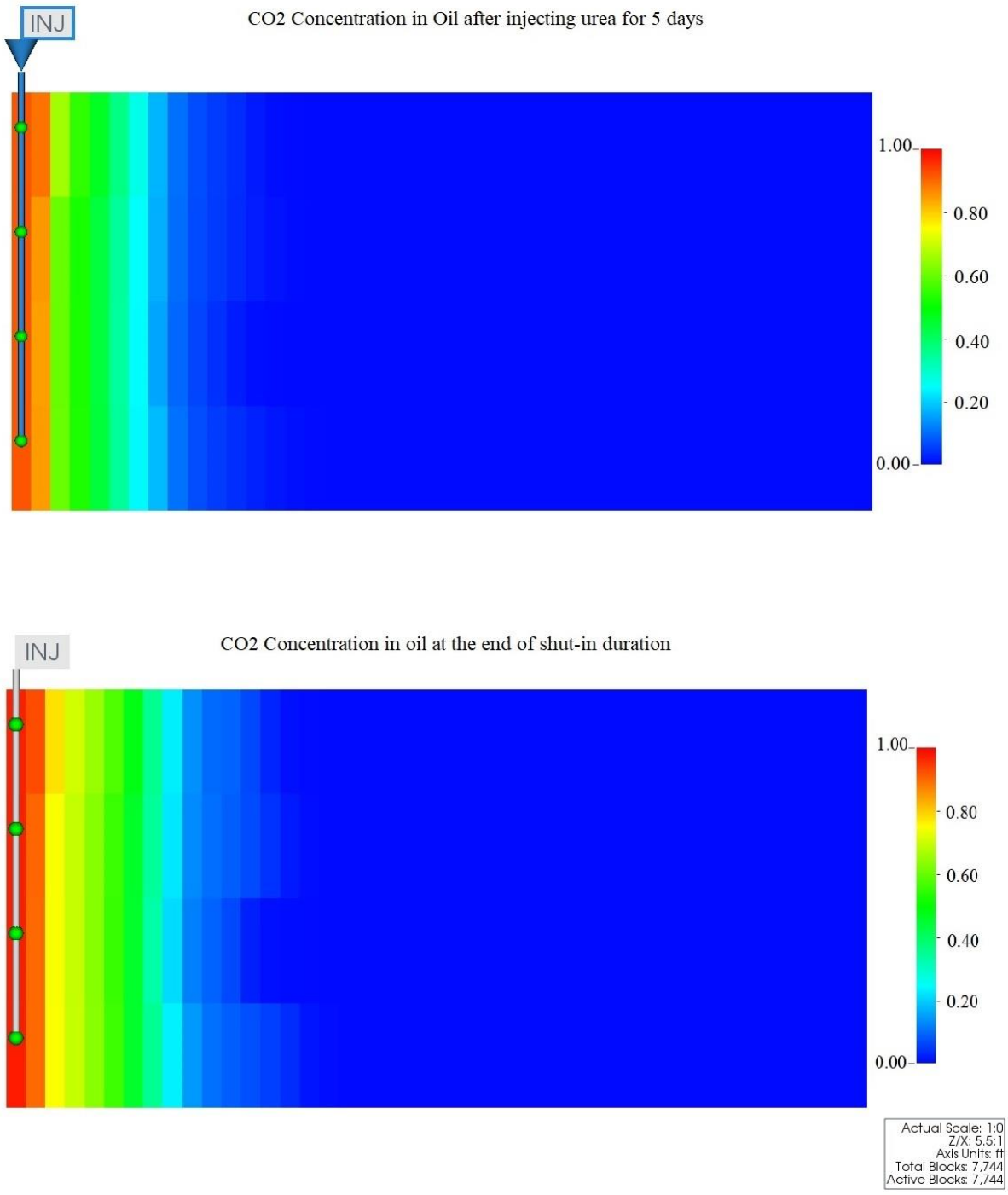

Figure 4-18 CO_2 concentration in oil after 5 days of urea injection and at the end of shut-in period

Chapter 5: Conclusions and Way Forward

Based on the study of the urea hydrolysis reaction, kinetics, equilibrium, different concentration, and mechanistic numerical model, validation of synergetic mechanism of ICE through history matching of laboratory experiments, and the upscaling of the1D mechanistic numerical model to 3D sector model, following conclusions were made:

5.1.Conclusions

- The synergetic mechanisms of ICE, 1) Oil swelling and viscosity reduction due to the generated CO_2 partitioning into the oil phase, and 2) Wettability change due to ammonia alkali, were successfully modeled and the objectives of the study were achieved.
- Based on urea reaction kinetics behavior in numerical simulation models, the reaction rate is highly sensitive to reservoir temperature, activation energy, and pre-exponential factor, and pH of brine in the reservoir. Adding alkali such as NaOH can improve the reaction rate.
- Gibbs free energy provided the minimum reservoir temperature for urea injection which is 70°C. Below this temperature, urea reaction will not be spontaneous and require catalysts such as sodium hydroxide to increase the reaction rate and make the urea reaction spontaneous. The reservoir temperature of 70°C should be one of the designing parameters for urea solution flooding.
- In designing ICE, urea decomposition and CO_2 generating rate are important factors to obtain a good EOR performance. If the reaction rate is slow, due to reservoir temperature or other factors, and injection rate must be slow or shut-in to give sufficient time for the reaction to generate sufficient CO_2. For low-temperature reservoirs, adding catalysis or

fine-tuning the injection scheme are important to avoid producing the urea at the offset production wells.

- According to the 1D mechanistic numerical model, the oil swelling is directly proportional to produced CO_2 mole by urea reaction and urea reaction is highly dependent on reaction kinetics. Also, the recovery factor by oil swelling and viscosity reduction was less than the oil swelling factor due to uncertainty in urea reaction kinetics. Therefore, it is recommended to acquire experimental data on oil swelling and urea reaction kinetics for different oil compositions during the In-Situ CO_2 experimental process.
- Ammonia alkali mechanism, also known as in-situ surfactant generation, was also modeled, but due to lack of evidence in terms of interfacial tension and relative permeability, the estimated recovery factor has high uncertainty.
- The ICE synergetic mechanisms of oil swelling, viscosity and IFT reduction, and wettability alteration were validated by history matching the three laboratory experiments and quantified the contributions of these mechanisms in terms of recovery factors.
- For the simulated cases, the incremental recovery due to oil swelling and viscosity reduction ranged between 6.4% to 18% and incremental recovery due to IFT reduction and wettability alteration ranged between 24% to 38%. The viscosity reduction of dodecane, Earlsboro oil and DeepStar oil were 76%, 79%, and 91%, respectively.
- Based on viscosity reduction in laboratory numerical mechanistic models, it was observed that viscosity reduction was higher in heavy oil compared to light oil; viscosity reduction in Test-1 was 76% whereas in Test-3 was 91%.

- The relative permeability of oil and water and endpoints were the most uncertain parameters while history matching the ICE laboratory experiments. The produced CO_2 moles increased by modifying the endpoint saturations and relative permeability to oil and water which may be due to more mobile oil in the porous media. However, this needs to be investigated further through laboratory experiments.
- Measured oil saturation vs. pore volume injected was matched well but, in some cases, they were mismatched due to cyclic injection of urea and water and CO_2 concentration dependency of relative permeability on different phases. However, the simulator does not accommodate the CO_2 concentration dependency of relative permeability and therefore, it was modified manually. Therefore, it is also recommended to measure the relative permeability for ICE experiments in the laboratory to further understanding the flow behavior of different fluids in the porous media.
- Molecular diffusion was not considered while history matching the laboratory experiments and validating ICE synergetic mechanisms.
- 1D mechanistic and laboratory numerical models were upscaled to a 3D sector model and the performance of ICE in terms of recovery on a field scale was evaluated. The optimum scenario was selected based on sensitivity analysis of injection rate, urea concentration, shut-in/No shut-in, and reservoir temperature. The optimum scenario was based on cyclic injection of urea, followed by shut-in (both injector and producer were shut-in) and brine injection. The urea injection slug, shut-in duration, brine injection slug was optimized based on incremental oil recovery and lesser injection of urea as compared to waterflooding base case.

- For the modeled sector model, the simulated optimum recovery was obtained with 25 wt.% urea concentration, urea slug size of five days, shut-in duration of five days and brine injection for forty days. In this scenario, 0.12 PV of water and urea recovered 3.48% incremental oil compared to waterflooding which recovered 9.79% oil with 0.10 PV of water injection, and continuous 25 wt.% urea injection recovered 5.52% incremental oil as compared to waterflooding with 0.13 PV of water and urea injection.

5.2. Way Forward

- Urea reaction kinetics with different catalysts at different temperatures should be studied to evaluate the potential of In-situ CO_2 EOR for low-temperature reservoirs.
- Relative permeability and oil swelling factor should be measured in the laboratory to reduce uncertainty in quantifying the recovery factors for different synergetic mechanisms of ICE.
- A field trial must be set up to study the ICE recovery under reservoir heterogeneities.
- Urea injection scheme must be optimized for a field trial based on reservoir heterogeneities and economic evaluation of ICE for different oil reservoirs.
- A huff ‘n’ puff (HNP) scenario must be considered while designing the ICE for a field trial.

References

1. BP., Statistical Review of World Energy 2020 (69th edition). Bp. doi: https://www.bp.com/content/dam/bp/business-sites/en/global/corporate/pdfs/energy-economics/statistical-review/bp-stats-review-2020-full-report.pdf
2. Frequently asked Questions (FAQs) - U.S. Energy Information Administration (EIA). (2020, September 11). Retrieved from https://www.eia.gov/tools/faqs/faq.php?id=847&t=6.
3. Lake, L. W. (2014). Fundamentals of enhanced oil recovery. Richardson, TX: Society of Petroleum Engineers.
4. Alvarado, V., & Manrique, E. (2010). Enhanced oil recovery: An update review. Energies, 3(9), 1529-1575. doi:10.3390/en3091529
5. Wang, S. (2018). Study and development of in-situ CO2 enhanced oil recovery (Published doctoral dissertation). University of Oklahoma.
6. Iqbal, G. M., & Satter, A. (2016). Chapter 16 Enhanced Oil Recovery. In Reservoir Engineering: The Fundamentals, Simulation, and Management of Conventional and Unconventional Recoveries. Gulf Professional Publishing.
7. IEA. (2018, November 01). Whatever happened to enhanced oil recovery? – analysis. Retrieved March 04, 2021, from https://www.iea.org/commentaries/whatever-happened-to-enhanced-oil-recovery.
8. Gbadamosi, A.O., Junin, R., Manan, M.A. et al. An overview of chemical enhanced oil recovery: recent advances and prospects. Int Nano Lett 9, 171–202 (2019). https://doi.org/10.1007/s40089-019-0272-8
9. Green, D. W., & Willhite, G. P. (2018). 7. Chemical Flooding. In *Enhanced oil recovery* (pp. 287-291). Richardson, TX, USA, Society of Petroleum Engineers.
10. Global Energy Institute. (2013). *CO2 Enhanced Oil Recovery* (Rep.). Institute for 21st Century Energy. doi: https://www.globalenergyinstitute.org/sites/default/files/020174_EI21_EnhancedOilRecovery_final.pdf
11. Verma, M.K., 2015, Fundamentals of carbon dioxide-enhanced oil recovery (CO2-EOR)—A supporting document of the assessment methodology for hydrocarbon recovery using CO2-EOR associated with carbon sequestration: U.S. Geological Survey Open-File Report 2015–1071, 19 p., http://dx.doi.org/10.3133/ofr20151071
12. Callahan, K., Goudarzi, L., Wallace, M., & Wallace, R. (2015). A review of the CO_2 pipeline infrastructure in the U.S. U.S. Department of Energy. doi:10.2172/1487233
13. Wang, S., Kadhum, M. J., Chen, C., Shiau, B., & Harwell, J. H. (2017). Development of in situ CO2 generation formulations for enhanced oil recovery. Energy & Fuels, 31(12), 13475-13486. doi: 10.1021/acs.energyfuels.7b02810
14. Li, K. (2018). Performance of UREA-BASED In-situ CO_2 EOR: Influences of Different porous media (published master's thesis). University of Oklahoma. doi: https://shareok.org/handle/11244/316321
15. Sparks, D. L. (2003). Chapter 7: Kinetics of Soil Chemical Processes. In Environmental Soil Chemistry (Second ed., pp. 207-244). New York: Academic Press.

16. Reaction Order. (2020, September 10). Retrieved March 10, 2021, from https://chem.libretexts.org/@go/page/1436
17. Sahu, J. N., Patwardhan, A. V., & Meikap, B. C. (2009). Equilibrium and kinetic studies of in SITU generation of ammonia FROM urea in a Batch reactor For flue GAS conditioning of thermal power plants. *Industrial & Engineering Chemistry Research, 48*(5), 2705-2712. doi:10.1021/ie801286h
18. Wang, S., Chen, C., Li, K., Yuan, N., Shiau, B., & Harwell, J. H. (2019). In situ CO2 enhanced oil recovery: Parameters affecting reaction kinetics and recovery performance. Energy & Fuels, 33(5), 3844-3854. doi: 10.1021/acs.energyfuels.8b03734
19. Kieke, M. L., Schoppelrei, J. W., & Brill, T. B. (1996). Spectroscopy of Hydrothermal Reactions. 1. The co2−h2o system and kinetics of Urea decomposition in AN FTIR Spectroscopy Flow Reactor Cell operable to 725 K and 335 bar. *The Journal of Physical Chemistry, 100*(18), 7455-7462. doi:10.1021/jp950964q
20. Simon, R., and D.J. Graue. "Generalized Correlations for Predicting Solubility, Swelling and Viscosity Behavior of CO2 -Crude Oil Systems." *J Pet Technol* 17 (1965): 102–106. doi: https://doi-org.ezproxy.lib.ou.edu/10.2118/917-PA
21. Or, C.., Sasaki, K.., Sugai, Y.., Nakano, M.., and M, Imai. "Swelling and Viscosity Reduction of Heavy Oil by CO_2-Gas Foaming in Immiscible Condition." *SPE Res Eval & Eng* 19 (2019): 294–304. doi: https://doi.org/10.2118/179738-PA
22. Fakher, S., & Imqam, A. (2020). A simplified method for experimentally quantifying crude oil swelling during immiscible carbon dioxide injection. *Journal of Petroleum Exploration and Production Technology, 10*(7), 3031-3042. doi:10.1007/s13202-020-00867-8
23. Hu, R., Crawshaw, J. P., Trusler, J. P., & Boek, E. S. (2016). Rheology and phase behavior of carbon dioxide and crude Oil Mixtures. *Energy & Fuels, 31*(6), 5776-5784. doi: 10.1021/acs.energyfuels.6b01858
24. Chung, Frank T.H., Jones, Ray A., and Hai T. Nguyen. "Measurements and Correlations of the Physical Properties of CO2-Heavy Crude Oil Mixtures." *SPE Res Eng* 3 (1988): 822–828. doi: https://doi-org.ezproxy.lib.ou.edu/10.2118/15080-PA
25. Barclay, T. H., & Mishra, S. (2016). New correlations for co2-oil solubility and viscosity reduction for light oils. *Journal of Petroleum Exploration and Production Technology, 6*(4), 815-823. doi:10.1007/s13202-016-0233-y
26. Urea. (n.d.). Retrieved March 16, 2021, from https://webbook.nist.gov/cgi/cbook.cgi?ID=C57136&Mask=2.
27. GIBBS free energy and the nature of chemical reactions. (n.d.). from http://www.tiem.utk.edu/~gross/bioed/webmodules/GibbsEnergy.htm#:~:text=A%20chemical%20reaction%20will%20have,from%20higher%20to%20lower%20energy.
28. Urea. (n.d.). Retrieved from https://webbook.nist.gov/cgi/cbook.cgi?Name=urea&Units=SI.
29. Li, K. (2018). Performance of UREA-BASED In-situ CO_2 EOR: Influences of Different porous media (published master's thesis). University of Oklahoma. doi: https://shareok.org/handle/11244/316321

30. Yuan, N. (2018). Improved surfactant performances in porous media: effects of hydrotropes and bio-olsovents (published master's thesis). University of Oklahoma. doi: https://hdl.handle.net/11244/316311

Appendix-1

Component	AVISC (cp)	(kPa-day)	(kPa-hr)	BVISC (K,C)	(F,R)
H2O	0.0047352	5.48E-14	1.32E-12	1515.7	2728.2
H2S	0.0084969	9.83E-14	2.36E-12	789.3	1420.7
N2	0.0110386	1.28E-13	3.07E-12	207.92	374.26
O2	0.0216926	2.51E-13	6.03E-12	197.29	355.11
CO	0.0119257	1.38E-13	3.31E-12	216.58	389.85
CO2	0.0007573	8.76E-15	2.10E-13	1331.1	2395.9
CH4	0.0104328	1.21E-13	2.90E-12	262.82	473.07
C2H6	0.0229832	2.66E-13	6.38E-12	360.58	649.05
C3H8	0.0214257	2.48E-13	5.95E-12	512.72	922.89
C4H10	0.0219066	2.54E-13	6.08E-12	612.12	1101.8
C5H12	0.0191041	2.21E-13	5.31E-12	722.23	1300
C6H14	0.0177073	2.05E-13	4.92E-12	835.35	1503.6
C7H16	0.0132383	1.53E-13	3.68E-12	1005.6	1810.1
C8H18	0.0131242	1.52E-13	3.65E-12	1090.7	1963.3
C9H20	0.0117124	1.36E-13	3.25E-12	1210.1	2178.3
C10H22	0.0115577	1.34E-13	3.21E-12	1286.2	2315.2
C12H26	0.0104376	1.21E-13	2.90E-12	1454.4	2617.9
C15H32	0.0095777	1.11E-13	2.66E-12	1654.4	2978
C17H36	0.0096344	1.12E-13	2.68E-12	1745.1	3141.1
C18H38	0.0095671	1.11E-13	2.66E-12	1790	3222.1
C20H42	0.0095545	1.11E-13	2.65E-12	1868.1	3362.5